Journal of Materials Chemistry A

ROYAL SOCIETY OF CHEMISTRY

REVIEW

View Article Online
View Journal | View Issue

Cite this: J. Mater. Chem. A, 2026, 14, 4323

Engineering MOFs for thin-film and nanofilm nanocomposite membranes for CO_2 separation

Farhang Pazanialenjareghi, Shweta Singh, Fathy Attia, Venkat Sainath Reddy Munnangi, Emmanuel M. Nsengiyumva, Yang Jiao and Haiqing Lin *

Received 28th September 2025
Accepted 6th December 2025

DOI: 10.1039/d5ta07953e

rsc.li/materials-a

Microporous crystalline metal–organic frameworks (MOFs) have been incorporated into polymers to enhance carbon capture performance due to their well-controlled pore sizes and porosity. However, MOFs may aggregate in the polymers and form interfacial voids, resulting in reduced selectivity. Such challenges are exacerbated when they are incorporated into thin-film nanocomposite (TFN) or nanofilm nanocomposite (NFN) membranes, where the effects of interfacial interactions and nanoconfinement become more pronounced in defect-free films as thin as <100 nm. To address these issues, novel MOFs have been developed to improve their distribution in thin films and their contribution to gas separation properties, such as surface functionalization, defect engineering, amorphization, and incorporation with polymers and macrocycles. We critically assess these strategies and highlight their contributions to enhancing CO_2 separation properties. Understanding the scaling and integration of these engineered MOFs in TFNs provides insights into designing next-generation membranes for molecular and ion separations.

1. Introduction

Membrane technology has emerged as one of the leading processes for carbon capture, reducing CO_2 emissions into the atmosphere, due to its high energy efficiency, lack of chemical waste, compact design, and simplicity in operation and maintenance.[1,2] Industrial membranes are usually made of polymers because they are low-cost and easy to process.[3,4] However, their separation performance often suffers from a trade-off between permeability and selectivity, *i.e.*, polymers with higher permeability tend to exhibit lower selectivity.[5] To address this, polymers are incorporated with nanofillers featuring well-controlled nanopores and unique separation properties, synergizing the advantages of both polymers and nanofillers.[6,7] Particularly, crystalline metal–organic frameworks (MOFs) formed by the self-assembly of metal ion clusters and organic ligands have attracted substantial attention,[8,9] due to their great flexibility of metal ions and ligands in designing desirable micropores in achieving superior gas separation properties.[10–13]

Significant progress has been made in developing mixed matrix freestanding films (MMFs, >10 μm) with superior gas separation properties, and several challenges have been identified. First, conventional MOF nanoparticles (NPs) can aggregate in polymers due to incompatibility, forming non-selective interfacial voids and thereby reducing gas selectivity.[11,14–16] Second, polymer chains may penetrate into and around the

Department of Chemical and Biological Engineering, University at Buffalo, The State University of New York, Buffalo, NY 14260, USA. E-mail: haiqingl@buffalo.edu

Farhang Pazanialenjareghi

Farhang Pazanialenjareghi is a PhD candidate in the Lab of Innovative Membranes under the guidance of Prof. Haiqing Lin at the University at Buffalo, SUNY. His current research focuses on developing thin-film nanocomposite (TFN) membranes with metal–organic frameworks (MOF-based TFNs) for gas separation applications.

Shweta Singh

Shweta Singh is a PhD candidate in the Lab of Innovative Membranes under the guidance of Prof. Haiqing Lin at the University at Buffalo, SUNY. She received her B. Tech in Chemical Engineering from Ahmedabad University, Gujarat, India, in 2018 and her M.S. in Chemical Engineering from University at Buffalo in 2023. Her current research focuses on developing polyamine-based sorbent materials for direct air capture of CO_2.

porous structure of MOFs and become rigidified, decreasing gas separation efficiency.[17] Finally and most importantly, industrial membranes often comprise selective layers as thin as <100 nm to achieve high gas permeance,[18–20] and the scalable production of defect-free thin-film (<1000 nm) nanocomposite (TFN) and nanofilm (<100 nm) nanocomposite (NFN) membranes with controlled distribution of MOFs remains a significant hurdle.[15,21–23]

Extensive strategies have been adopted to engineer MOFs that address the aforementioned challenges, such as fine-tuning pore sizes and surfaces, enhancing gas separation properties, and achieving uniform dispersion in polymers.[10,24–26] First, the surface of MOFs can be modified with functional groups (SM-MOFs), such as amines[27–29] and ionic liquids (ILs),[30,31] to introduce affinity towards polymers; and *in situ* growth of MOFs and *in situ* polymerization of polymers were used to enhance the dispersibility of MOF NPs.[32,33] Second, defects can be introduced to MOFs, resulting in defect-engineered MOFs (DE-MOFs)[34–36] and even amorphous MOFs (aMOFs).[37–39] Third, MOF structures can be functionalized by polymers (polyMOFs)[40,41] and macrocycles (MC-MOFs);[42–44] and MOFs with unique morphologies (such as wrinkled surfaces) have been synthesized.[45]

Various aspects of the MMFs containing MOFs have been reviewed in the literature, such as *in situ* synthesis of MOFs and polymers,[32] engineering interfacial compatibility,[11,33] scalability and stability,[46] and H_2 separations.[47] MMFs based on advanced MOFs such as DE-MOFs,[26,35] aMOFs,[48,49] and post-modified MOFs[50] were also summarized. Furthermore, TFN membranes based on conventional MOFs and SM-MOFs have also been reviewed for various gas and liquid separations.[15,48,51]

Fathy Attia

Fathy Attia is a PhD candidate in Chemical and Biological Engineering at the University at Buffalo in Prof. Haiqing Lin's lab of Innovative Membranes. He received his B.S. in Chemistry and M.S. in Organic Chemistry from Mansoura University, Egypt, in 2010 and 2016, respectively. His current research interest focuses on polymer synthesis and polymer/MOF Mixed-Matrix Materials (MMMs) for gas separation membranes.

Venkat Sainath Reddy Munnangi

Venkat Sainath Reddy Munnangi is a Master student in Chemical and Biological Engineering at the University at Buffalo. He earned his Bachelor's degree in Chemical Engineering from Jawaharlal Nehru Technological University in 2021. Under the Supervision of Prof. Haiqing Lin, his research focuses on the surface modification of membranes used for post–combustion carbon capture.

Emmanuel M. Nsengiyumva

Emmanuel M. Nsengiyumva earned his PhD in Chemical Engineering from the University at Buffalo in 2023. After completing his PhD, he was awarded a prestigious National Science Foundation (NSF) ASCEND postdoctoral research fellowship for three years, under the joint mentorship of Professors Chong Cheng and Haiqing Lin. His NSF project focuses on developing materials that feature nanopores and can self-heal when damaged for gas separation. Currently, supported by a PRO-DiG+ fellowship, his research focuses on designing and synthesizing innovative polymeric materials for various applications.

Yang Jiao

Yang Jiao received his PhD in Chemistry from the University of Science and Technology of China in 2024. He is currently a post-doctoral researcher at the University at Buffalo, SUNY, working under the supervision of Prof. Haiqing Lin. His research focuses on membrane-based gas separation.

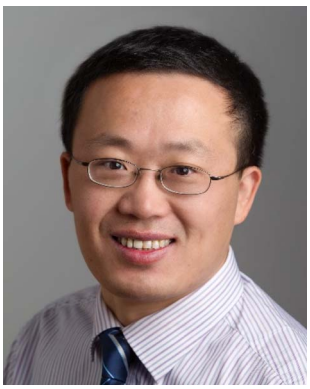

Haiqing Lin

Haiqing Lin Dr Haiqing Lin received his PhD in Chemical Engineering from the University of Texas at Austin in 2005 and then joined Membrane Technology and Research, Inc. (MTR) as a Senior Research Scientist. Afterwards, he joined the University at Buffalo (UB) as an assistant professor in 2013 and was promoted to professor in 2021. His research focuses on advanced polymeric membranes for gas separations, water purification, and ion separations, elucidating the relationships of chemical structures, nanostructures, and transport behaviors of small penetrants. He has published nearly 175 peer-reviewed articles and book chapters, and he is a co-inventor of 10 US patents and patent applications.

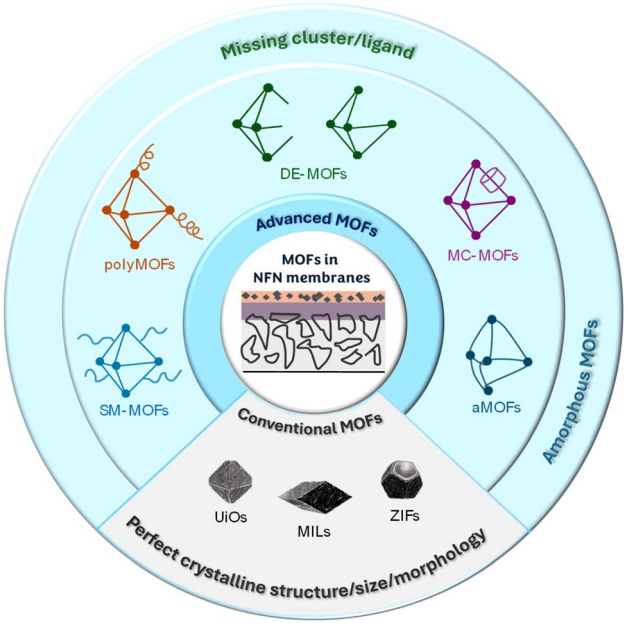

Fig. 1 Summary of MOF-based TFN and NFN membranes for CO_2 separations, including conventional MOFs (like UiOs, ZIFs, and MILs) and engineered MOFs, such as SM-MOFs, DE-MOFs, aMOFs, polyMOFs, and MC-MOFs.

This paper provides a comprehensive and critical review of the state-of-the-art MOF-based TFN membranes with superior CO_2 separation performance, highlighting the role of the engineered MOFs in fabricating nanocomposite membranes with enhanced separation performance (Fig. 1). We first describe the gas transport model in TFN and NFN membranes and highlight the leading ones containing conventional MOF NPs with good CO_2 separation properties. Second, advanced MOFs engineered to improve membrane CO_2 separation properties are critically reviewed, such as SM-MOFs, DE-MOFs, aMOFs, polyMOFs, MC-MOFs, and 2D MOFs. Third, the effect of the engineered MOFs on membrane separation properties is systematically compared, and the large-scale production of TFN membranes is discussed. Finally, we provide our perspectives on the future direction of developing this exciting membrane platform for practical gas separations. Elucidating interactions between these advanced MOFs and polymers may help design nanocomposites for other applications, such as membranes for electrochemical devices, coatings, sensors, and structured materials.

2. Conventional MOF-based TFN membranes

This section introduces the rationale of incorporating conventional MOFs to enhance CO_2 separation properties, as well as conventional methods for fabricating TFN membranes.

2.1. Gas transport models

Gas transport through polymeric materials (like MMFs) usually follows a solution-diffusion mechanism, and gas permeability (P_A) can be expressed as:

$$P_A = S_A \times D_A \quad (1)$$

where S_A is gas solubility, and D_A is the average gas diffusion coefficient in the materials. Gas permeability has units of Barrer, where 1 Barrer $= 10^{-10}$ cm^3(STP) cm cm^{-2} s^{-1} cmHg^{-1}.

TFN membranes are characterized by gas permeance (Q_A). Q_A has units of GPU, where 1 GPU $= 10^{-6}$ cm^3(STP) cm^{-2} s^{-1} cmHg^{-1}. The ideal permeance ($Q_{A,ideal}$) is determined by the selective layer and given by:

$$Q_{A,ideal} = P_A/l \quad (2)$$

where l is the selective layer thickness.

Various models have been developed to describe gas permeability in the MMFs. For example, the Lewis–Nielsen model is valid with the filler loading (φ_d) up to 64 vol%. The gas permeability of MMFs (P_M) can be expressed in eqn (3):[52]

$$\frac{P_M}{P_P} = \frac{1 + 2\varphi_d(\gamma - 1)/(\gamma + 2)}{1 - \Psi\varphi_d(\gamma - 1)/(\gamma + 2)} \quad (3)$$

where P_P is the permeability of the continuous polymer phase, and γ is the permeability ratio of the MOF to the polymer. The parameter of Ψ is defined in eqn (4):

$$\Psi = 1 + \left(\frac{1 - \phi_m}{\phi_m^2}\right)\varphi_d \quad (4)$$

where ϕ_m is the maximum packing volume fraction and is often taken as 64 vol% for random close packing of uniform spheres. If the γ value is much greater than 1 due to the high porosity of the MOFs, eqn (3) can be reduced to:

$$\frac{P_M}{P_P} = \frac{1 + 2\varphi_d}{1 - \Psi\varphi_d} \quad (5)$$

Eqn (5) predicts that introducing a highly permeable discontinuous phase in a polymer can increase permeability without affecting gas selectivity.

The Maxwell model has also been widely used to estimate gas permeability in MMFs (φ_d < 20%). At γ >> 1, the model can be reduced to the following equation:

$$\frac{P_M}{P_P} = \frac{1 + 2\varphi_d}{1 - \varphi_d} \quad (6)$$

However, as both Lewis–Nielsen and Maxwell models do not consider the morphology and distribution of MOFs and their interfacial incompatibility with polymers, they only provide general guidance and lack accuracy in quantitative prediction.[52,53]

2.2. Resistance model and geometric restriction in membranes

Fig. 2 displays schematic diagrams of gas permeation through thin-film composite (TFC) and TFN membranes.[2,52] Gutter layers are typically used to prevent the pore penetration of the coating solution into the porous support and to provide a smooth surface for coating the selective layer.[19,54–56] In the absence of the effect from the porous support, gas permeation

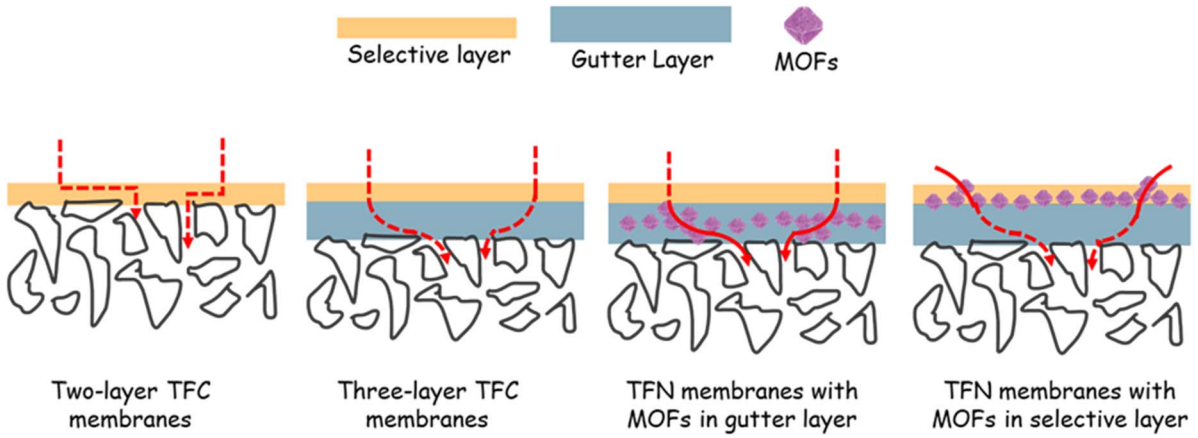

Fig. 2 Scheme of gas permeation through multi-layer TFC and TFN membranes, including MOFs in the gutter and selective layers.

through the membranes can be estimated using a resistance-in-series model:

$$1/Q_A = 1/Q_{A,ideal} + (l/P_A)_G \quad (7)$$

However, the porous support often exerts significant geometric restriction,[19,20] where gas molecules prefer to diffuse through the surface pores of the porous support, thus increasing the diffusion path. Toward this, the permeation efficiency (β_A) is defined to represent the effect of the gutter layer and the surface pore size and porosity of the porous support:[57,58]

$$\beta_A = \frac{Q_A}{Q_{A,ideal}} = \frac{Q_A}{(P_A/l)} \quad (8)$$

The β_A values can be estimated from computational fluid dynamics (CFD) simulations.

2.3. Typical polymers and methods to fabricate TFN membranes

Fig. 3 shows typical materials used to construct TFN membranes.[2,52] Porous supports can be made of polyvinylidene fluoride (PVDF), polysulfone (PSF), and polyacrylonitrile (PAN), which have low costs and good processability. Gutter layers can

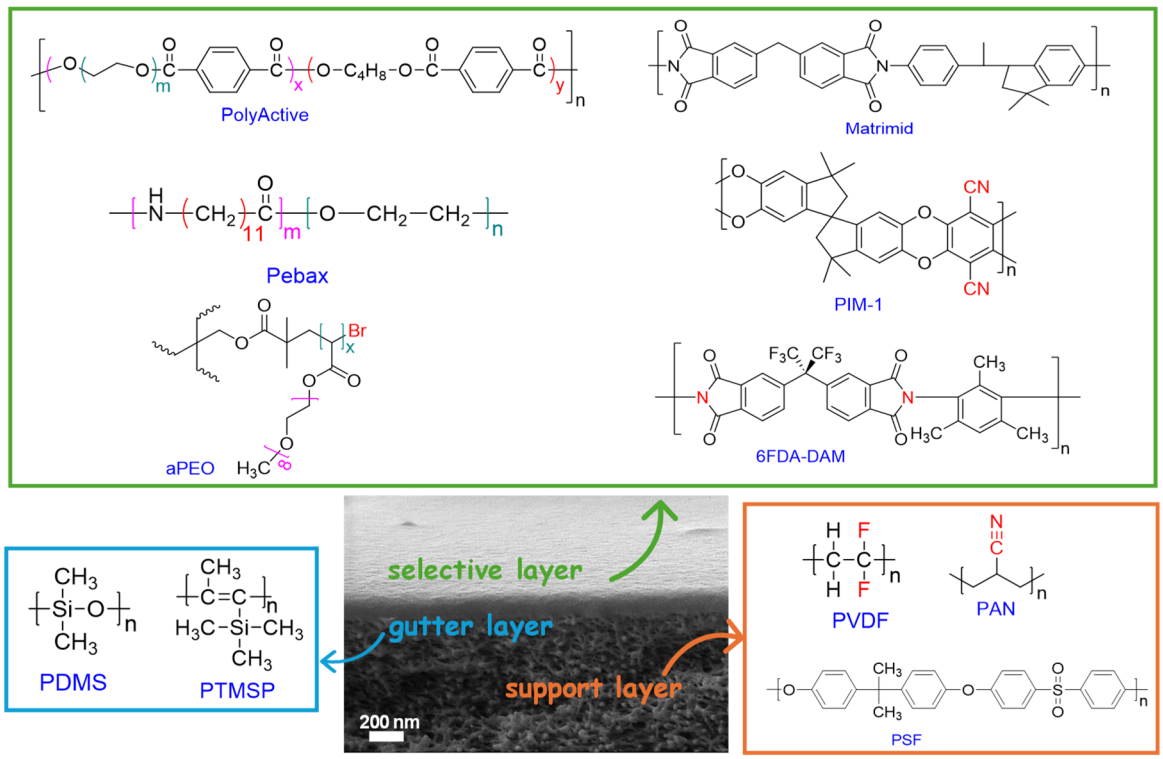

Fig. 3 Configurations of TFN membranes, and chemical structures of typical polymers, gutter layers, and porous supports.

be made of polydimethylsiloxane (PDMS) and poly(1-trimethylsilyl-1-propyne) (PTMSP), which exhibit high gas permeability and excellent coatability.[19] Additionally, MOF nanosheets have been directly used as gutter layers,[59,60] and MOFs have been incorporated into the PDMS layer to enhance its permeance.[61,62] Several polymers have been widely employed for TFN membranes, including commercial poly(ethylene oxide) (PEO)-containing copolymers such as Pebax and PolyActive, amorphous PEO (*a*PEO), polymers of intrinsic microporosity (PIMs), and polyvinyl amine (PVAm).[54,55,63]

TFN membranes can be fabricated using conventional methods, including *in situ* growth and polymerization, interfacial polymerization (IP), dip coating, and spinning coating (Fig. 4a).[54,56,63] Novel approaches have also been demonstrated at a lab scale, including additive manufacturing (3D printing), continuous assembly of polymers (CAP), and spray coating (Fig. 4b).[64–67] For instance, PIM-1 containing HKUST-1 was deposited on PAN support using a 3D printing method (Fig. 4c),[68] and the layer thickness was varied between 2.5 μm and 400 nm by manipulating coating solution concentration and coating cycle. Fig. 4d presents the use of CAP to synthesize cross-linked PEO as thin as 30 nm on top of a MOF substrate, which exhibited CO_2 permeance of 3000 GPU with CO_2/N_2 selectivity of 34.[65]

2.4. TFN membranes based on conventional MOFs

Conventional TFN membranes are often prepared using conventional MOFs. Table 1 summarizes representative membranes with superior CO_2/N_2 or CO_2/CH_4 separation properties. Generally, adding MOFs increased both gas permeance and selectivity, and the effect depends on the NP surface chemistry. For example, MOF-808 exhibits large pores (4.8 and 18.4 Å) and unsaturated metal sites, providing high CO_2 adsorption capacity; adding 33 mass% MOF-808 (30–60 nm) in a PVAm selective layer (140 nm) increased CO_2 permeance by 100% from 1376 to 2753 GPU and CO_2/N_2 selectivity by 120% from 82 to 181.[69] Compatibilizers can be used to mitigate interfacial incompatibility. For instance, adding 10 mass% ionic liquid (IL) into nanofilms of ZIF-8 and a polymerizable ionic liquid (PIL) increased CO_2 permeance from 1056 to 1106 GPU and CO_2/N_2 selectivity from 22 to 27.[70]

The morphology and size of MOF NPs significantly impact their CO_2 separation properties. Furthermore, the incorporation of NPs in the nanofilms affects polymer chain dynamics, resulting in unexpected benefits, such as enhanced resistance to physical aging and increased polymer chain rigidity (and thus size-sieving ability). The details are described below.

2.4.1. Effect of the MOF morphology and size. The MOF morphology and size can be manipulated using modulators,

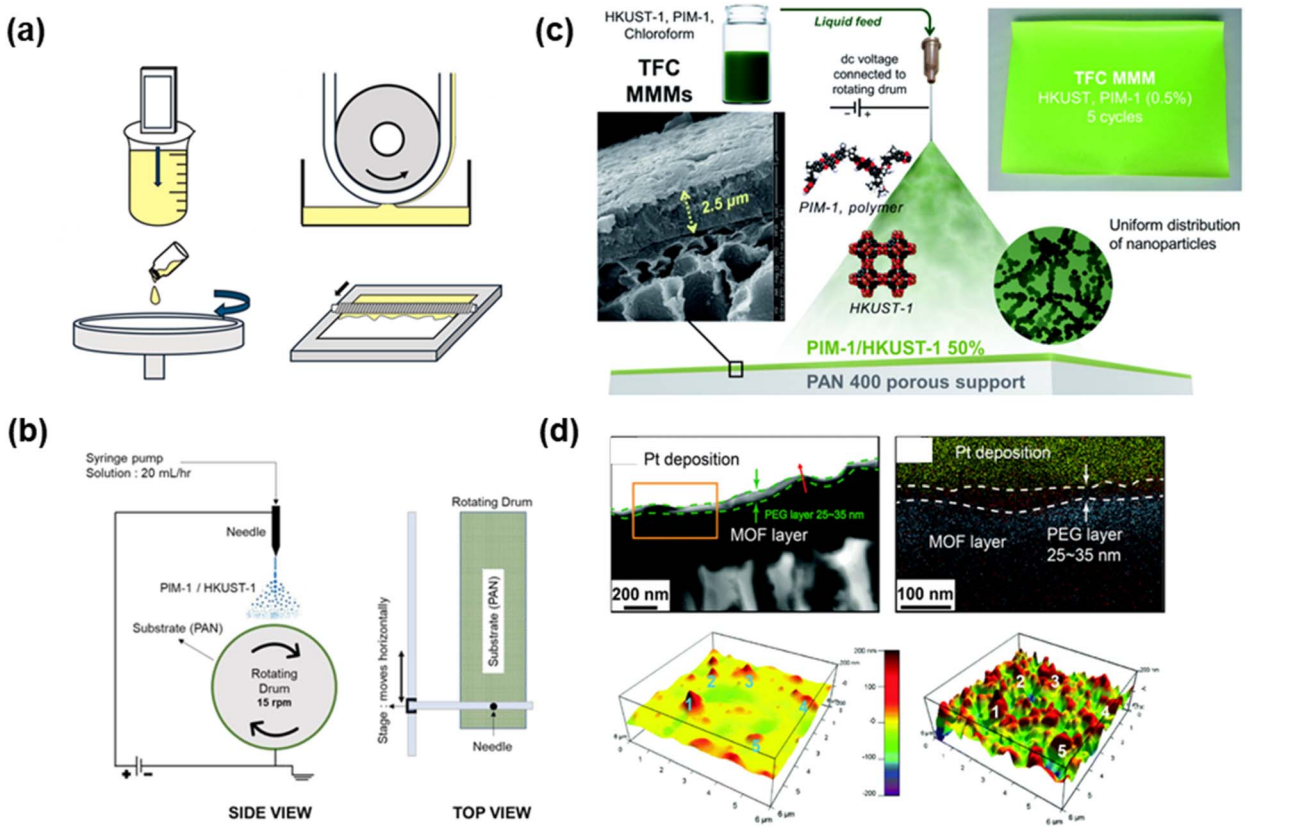

Fig. 4 Fabricating TFN membranes. (a) Common coating methods, including dip-coating (top left), kiss-coating (top right), spin-coating (bottom left), and bar-coating (bottom right).[55] Copyright 2025. Reproduced with permission from Elsevier. (b) Schematic of electrospray used for fabricating (c) membranes comprising PIM-1 and HKUST-1.[68] Copyright 2021. Reproduced with permission from the Royal Society of Chemistry. (d) Cross-sectional TEM and EDX mapping (top) and 3D AFM images (bottom) of membranes prepared by CAP.[65] Copyright 2018. Reproduced with permission from the Royal Society of Chemistry.

Table 1 Materials and CO_2 separation results of TFC membranes containing various conventional MOF NPs

	Selective layers							Selectivity		
Support/gutter layer	Polymer[a]	MOFs	Sizes (nm)	MOF (wt%)	l (nm)	T (°C)/ p (bar)	CO_2 permeance (GPU)	CO_2/ N_2	CO_2/ CH_4	Ref.
PSF/PDMS	*a*PEO	UiO-66-NH_2	45–85	0	178	23/2	1400	50		52
				10	200	23/2	2900	48		
PSF/PDMS	PVAm	MOF-808	30–60	0	—	25/2	1376	82		69
				33	145	25/2	2753	181		
PSF/PDMS	PA	ZIF-8	75	—	190	25/1.5	1600	35		71
				5	65	25/1.5	2740	104		
PSF/PTMSP	IL-Pebax	—		—	300	35/3	497	27		72
		ZIF-8	30	15	300	35/3	751	25		
		ZIF-94	48	15	300	35/3	819	25		
PSF	PBE	MOF-808	500–600	0	—	30/1	431	36		73
				40	350	30/1	1069	53		
PAN/PDMS@ aMOF	PIM-1	—		—	650	35/1	4320	19		74
		MOF-74-Ni	20–30	10	670	35/1	5018	31		
		UiO-66-NH_2	20–30	10	660	35/1	7460	26		
PSF/PTMSP	PTO	UTSA-16	6000	0	250	30/1	737	38	17	75
				10	300	30/1	1070	41	17	
PSF/PTMSP	PAP	ZIF-8	60	0	600	25/1	1056	22	10	70
				10	600	25/1	1017	33	13	
PSF/PTMSP	PVI-POEM	ZIF-8	100–200	0	300	30/1	1086	40	19	76
				50	300	30/1	4474	32	12	
PSF/PTMSP	PGO	—		—	600	25/1	889	31	15	77
		MIL-140C	0.2 × 2 μm	10	600	25/1	1364	40	22	
		UiO-67	200	10	600	25/1	1301	36	16	

[a] PA: polyamide; PBE: poly(2-[3-(2*H*-benzotriazol-2-yl)-4-hydroxyphenyl] ethyl methacrylate)-*co*-poly(oxyethylene methacrylate); PTO: poly(tetrahydrofurfuryl methacrylate)-*co*-poly(poly(oxyethylene methacrylate)); PAP: poly(1-allyl-3-methylimidazolium bis(trifluoromethanesulfonyl)imide-*co*-poly(ethylene glycol) methyl ether methacrylate); PVI-POEM: poly(vinyl imidazole)-poly(oxyethylene methacrylate); PGO: poly(glycidyl methacrylate)-*co*-poly(oxyethylene methacrylate).

which regulate the nucleation process and growth kinetics.[78–80] Modulators can either influence the acid/base equilibria of starting materials or compete with the ligands in the self-assembly of frameworks. For example, a modulator may increase the linker deprotonation, accelerating the crystal seed growth and thus decreasing the NP size;[78] increasing the acidity from acetic acid (pK_a = 4.76), formic acid (3.74), to trifluoroacetic acid (0.3) reduced the NP size from 200 to 30 nm.[81]

The particle size plays a critical role in their dispersibility and compatibility within polymers. Smaller NPs exhibit better dispersibility and higher interfacial surface areas, and thus, they are often preferred. For instance, MOF NPs with ~100 nm

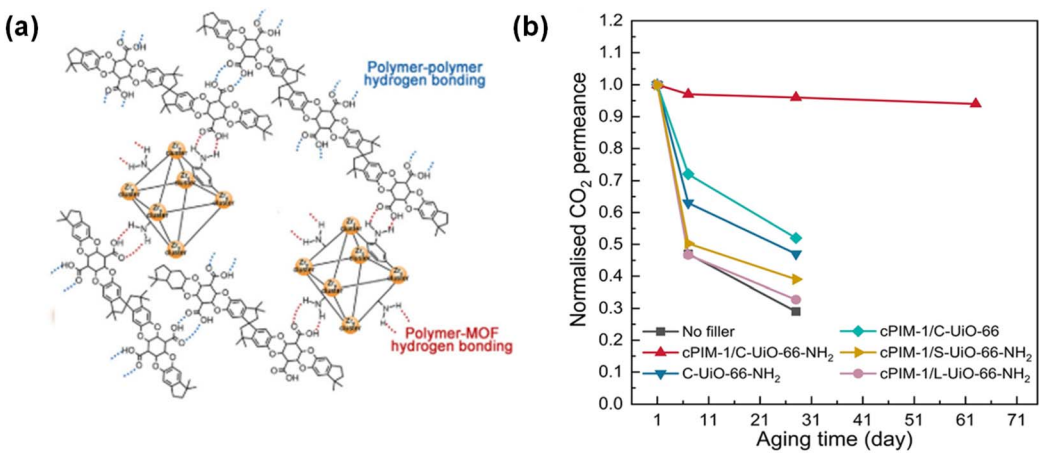

Fig. 5 TFN membranes with conventional MOF NPs for CO_2/N_2 separation. UiO-66-NH_2 to enhance resistance to physical aging in cPIM-1, including (a) scheme of H-bonds and (b) effect of the filler type on the normalized CO_2 permeance.[84] Copyright 2023. Reproduced with permission from John Wiley & Sons, Inc.

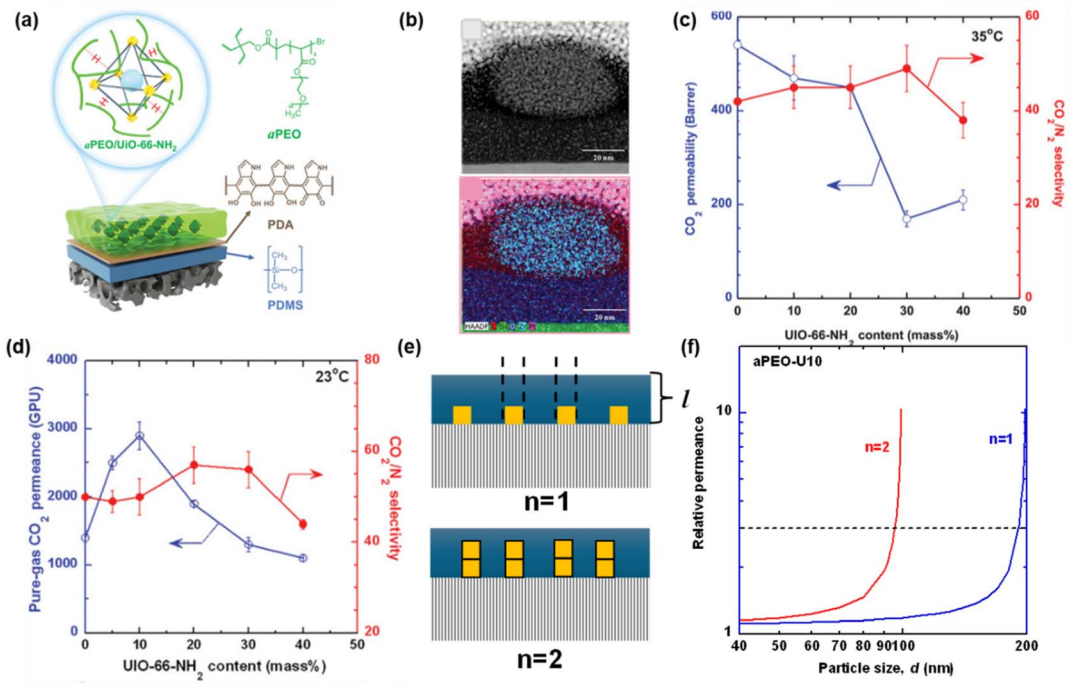

Fig. 6 Effect of nanoconfinement and NP distribution in TFN membranes based on UiO-66-NH_2 and *a*PEO. (a) Membrane configuration. (b) TEM images of nanofilms showing good interfacial compatibility. Comparison of CO_2/N_2 separation properties between (c) thick films (200 μm) and (d) nanofilms (~120 nm). (e) Schematic of the selective layer. (f) Permeance ratio (defined as Q_{Exp}/Q_{aPEO}) as a function of *d* and *n* values with 10 mass% UiO-66-NH_2. Copyright 2024.[52] Reproduced with permission from John Wiley & Sons, Inc.

were added into the PAN nanofiber supports, and then PIM/PU blends were spun-coated as selective layers (~180 nm) over a PDMS gutter layer; adding UiO-66-NH_2 increased CO_2 permeance from 1140 to 3690 GPU and CO_2/N_2 selectivity from 20 to 92.[82] Interestingly, micron-sized UTSA-16 particles (~6 μm) were dispersed in a copolymer (PTO) of ~300 nm; adding 30 wt% UTSA-16 increased CO_2 permeance from 700 to 1800 GPU and slightly decreased CO_2/N_2 selectivity from 38 to 32.[75]

Modulators can also be used to fine-tune MOF morphology. For instance, using monocarboxylic acid- and amine-based modulators can allow the growth of MOFs with different morphologies.[83] Specifically, nanocubes were obtained using both acetic acid and pyridine, and nanosheets were obtained when only the aminated modulator was used. Similarly, using benzoic acid and pyridine resulted in the formation of nanorods and nanoplates, respectively.

Zr-based MOFs with different morphologies have been investigated. For example, UiO-67 and MIL-140 have the same building blocks, while UiO-67 has a 3D shape with larger cages (12 and 23 Å), and MIL-140 has a rod shape with 9 Å pore sizes.[77] Adding 10 mass% MIL in PGO increased CO_2 permeance from 889 to 1364 GPU, CO_2/N_2 selectivity from 31 to 40, and CO_2/CH_4 selectivity from 15 to 22. By contrast, adding 10 mass% UiO increased CO_2/N_2 selectivity to 35 but barely affected CO_2/CH_4 selectivity. The discrepancy was attributed to the polymer's easier infiltration into the UiO-67 with its more open structures, which blocked gas permeation.

2.4.2. Enhanced resistance to physical aging by MOFs. PIMs are subject to physical aging, resulting in a rapid decrease in gas permeability over time, and the aging behavior is exacerbated for thinner films.[55] A strategy to mitigate aging is to introduce UiO-66-NH_2 (~10 nm) in carboxylated-PIM-1 (c-PIM-1). The hydrogen bonds (H-bonds) between the –NH_2 of the MOFs and the –COOH on the polymer enabled uniform dispersion of the NPs and reduced the polymer chain mobility (Fig. 5a), which in turn reduced aging over time.[84] Adding 8.5 mass% UiO-66-NH_2 reduced the loss of CO_2 permeance over 63 days from 71% to 6% while retaining CO_2/N_2 selectivity in a binary gas test (Fig. 5b).

2.4.3. Effect of nanoconfinement and NP distribution in the nanofilms. The nanofilms in the TFN membranes are often subject to nano-confinements, particularly when there are specific interactions between the polymer and nanofillers or between the nanofilms and substrates.[85,86] Such confinement may affect the packing of polymer chains or the distribution of MOF NPs, thereby influencing gas transport properties. For instance, UiO-66-NH_2 NPs were added to *a*PEO freestanding films (Fig. 6a), and they had excellent interfacial compatibility due to the H-bonds between the polar polymer and –NH_2 groups of the MOFs (Fig. 6b); however, gas permeability decreased with increasing the NP loading (Fig. 6c), which was attributed to the pore penetration and H-bonds.[52] By contrast, adding 10% NPs into the 120 nm-thick selective layer increased CO_2 permeance from 1400 to 2900 GPU while retaining CO_2/N_2 selectivity of 49 (Fig. 6d).

To estimate the effect of the NPs on the gas permeance of the membrane, the NPs were assumed to be uniform cubes with a length of *d* (nm) and an infinite gas permeance (Fig. 6e). The

experimental gas permeance of the membrane (Q_{Exp}) can be estimated using the resistance in parallel model, and the following equation was derived:

$$Q_{Exp}/Q_{a\mathrm{PEO}} = 1 + \varphi_d \frac{1}{1 - nd} \quad (9)$$

where $Q_{a\mathrm{PEO}}$ is the gas permeance of the pure *a*PEO, and n is the number of particles stacked vertically. Fig. 6f shows the relative permeance (defined as $Q_{Exp}/Q_{a\mathrm{PEO}}$) as a function of the d and n values. With the particle size of 45–85 nm, an n value of 2 resulted in the relative permeance remarkably close to the experimental result (3.0) for the *a*PEO-U10 membrane. The consistency between the simulation and experimental results further validates the importance of the particle distribution in the nanofilms for gas transport.

3. TFN membranes based on engineered MOFs

MOFs have been molecularly engineered to improve their compatibility with polymers, distribution in nanofilms, and gas separation properties. This section focuses on recently emerged MOFs, including SM-MOFs, DE-MOFs, aMOFs, polyMOFs, 2D MOFs, and others with unique morphologies.

3.1. TFN membranes based on SM-MOFs

The surface of MOFs can be modified using a covalent or coordinative approach,[50,87,88] as summarized in Table 2. For example, polymethylmethacrylate (PMMA), polyurethanes, and polyimides were used to modify the surface, improving interfacial compatibility and MOF dispersibility, as well as enhancing gas separation performance.[89–95] Specifically, UiO-66-NH_2 reacted with the dianhydride end groups of 6FDA-Durene oligomers, reducing the MOF agglomeration;[93] ZIF-8 NPs were modified with a shell of poly(1,3-dioxolanne) methacrylate (PDXLMA) and fabricated into TFN membranes, leading to CO_2 permeance of 3969 GPU and CO_2/N_2 selectivity of 28.[96] Additionally, unsaturated metal ions/clusters can be coordinated *via* chemicals containing functional groups like amines. For example, tetraethylenepentamine (TEPA) was used to modify Mg-MOF-74, where TEPA coordinated with the unsaturated Mg^{2+} centers, enhancing their dispersibility.[97]

Fig. 7a shows that UiO-66 MA NPs were copolymerized *in situ* with poly(ethylene glycol) methyl ether methacrylate (PEGMEMA) and dimethylsiloxane-ethylene oxide copolymer (PEODMS), forming a covalently crosslinked MOF–polymer network.[98] This strategy enabled high MOF loadings (40 wt%) without aggregation within 100 nm-thick selective layers (Fig. 7b). Adding 40% filler achieved CO_2 permeance of 3067 GPU while retaining CO_2/N_2 selectivity of 26. By contrast, UiO-66-NH_2 was directly dispersed in the polymer to form membranes (h-UiO-66-MA@P), which exhibited CO_2/N_2 selectivity decreasing with increasing MOF loading, highlighting the effectiveness of the covalent bonding between the polymer and MOFs.

Fig. 7c illustrates the affinity between amine-functionalized ZIFs and PIs, enabling the fabrication of TFN membranes with a thickness of ~200 nm.[101] Adding 20 wt% NH_2-ZIFs increased CO_2 permeance by 156% to 778 GPU with CO_2/N_2 selectivity by 55% to 34. In another study, functionalized UiO-66 NPs (50–150 nm) were used to fabricate 100 nm-thick NFN membranes (Fig. 5e).[99] UiO-66-Br and UiO-66-NO_2 provided higher CO_2 sorption capacity and better interfacial compatibility than UiO-66, and adding 40 wt% UiO-66-Br or UiO-66-NO_2 increased CO_2 permeance from 1393 to 1900 GPU and CO_2/N_2 selectivity from 23 to 37 (Fig. 5f).

3.2. TFN membranes based on DE-MOFs

DE-MOFs can increase surface area, tune pore volume and structure, and provide metal and ligand changes.[35,102–104] They are often prepared by *de novo* and post-synthesis treatment.[80,105] In the *de novo* approach, defects are generated during MOF formation by regulating synthesis conditions, such as ligand composition and solution temperature. Particularly, using two or more ligands in a starting solution introduces competition

Table 2 Materials and CO_2 separation results of TFN and NFN membranes containing SM-MOF NPs

		Selective layers							Selectivity		
Membranes	Support/gutter layer	Polymers	MOFs	Size (nm)	MOF (wt%)	l (nm)	T (°C)/p (bar)	CO_2 permeance (GPU)	CO_2/N_2	CO_2/CH_4	Ref.
NFN	PAN	PEGMEA-PEODMS	c-UiO-66 MA	40–50	0	100	25/1	1450	25		98
					40	100		3076	26		
	PSf/PTMSP	PGO	—		—	80	25/1	1393	23	10	99
			UiO-66	50–150	20	100		1555	35	14	
			UiO-66-Br	50–150	20	70		1703	37	14	
			UiO-66-NO_2	50–150	20	80		1816	37	14	
TFN	PAN	ZIF-8/PDXLAMA$_{1h}$		444		350	25/1	6035	21		96
		ZIF-8/PDXLAMA$_{2h}$		991		630		3969	28		
	PSF/PTMSP	Pebax	—		0	600	35/3	181	43	19	100
			UiO-66-NH_2	4	5	700		277	45		
			UiO-66-NO_2	6	5	700		155	51		
	PAN/PDMS	PI	NH_2-ZIF-8	82	0	300	30/1	304		22	101
					20	140		778		34	

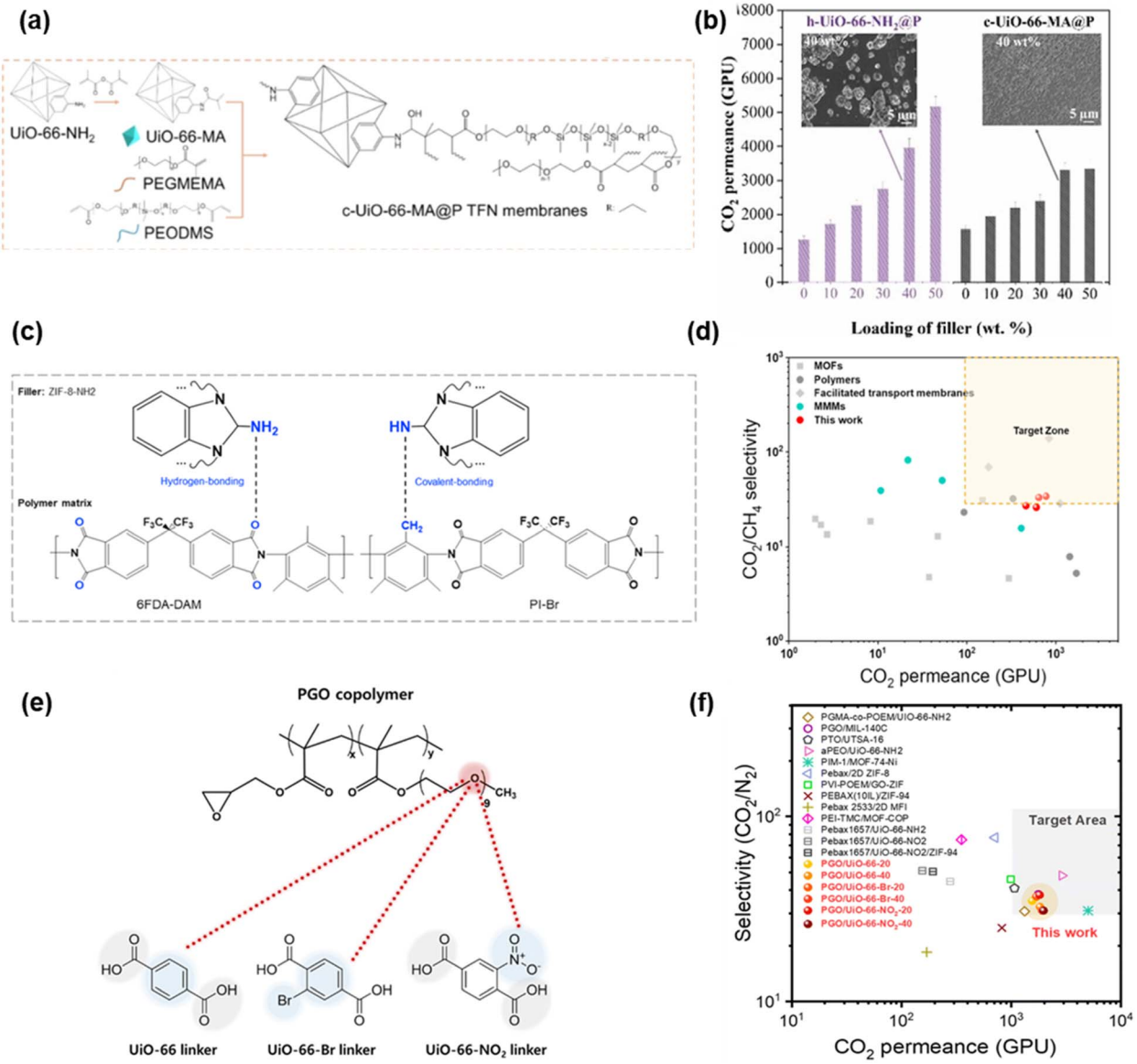

Fig. 7 TFN membranes based on SM-MOFs. (a) Scheme of *in situ* copolymerization of UiO-66-MA and PEGMEMA, and (b) effect of MOF loadings on CO_2 permeance.[98] Copyright 2024. Reproduced with permission from John Wiley & Sons, Inc. (c) Scheme of bonding between amine ZIF-8 and PIs and (d) gas separation properties.[101] Copyright 2023. Reproduced with permission from Elsevier. (e) Scheme of interaction between the polymer and UiO ligands and (f) gas separation properties.[99] Copyright 2025. Reproduced with permission from the Royal Society of Chemistry.

between ligands to coordinate with metal ions, resulting in defects due to unmatched crystal structures.[106,107] For example, adding a thermally labile ligand to the MOFs before thermal treatment at the decomposition temperature induced structures with missing ligands;[105] amino benzoic acid was added to terephthalic acid, resulting in defective sites and introducing amino groups with affinity towards CO_2.[105] This method is also influenced by other factors, such as mixed metal sources, solvent types, and other synthesis methods (like microwave).[80,107]

For the method of post-synthesis treatment, MOFs are post-modified by exchanging ligands or metal centers, a process also known as post-synthesis exchange (PSE).[50,87,88] The coordination of metal–ligand is kinetically unstable, allowing for breakage or reformation within a MOF lattice.[50,88] Fig. 8a and b illustrates the metal or ligand exchange by adding a new metal or ligand, respectively. For instance, a bimetallic Zr/Ti-based MOF was synthesized with high CO_2 adsorption capacity, and more stable MOFs were prepared by complete metal exchange of Zn^{2+} with Cu^{2+}.[108,109] The ligand exchange can be achieved by exposure to a ligand-concentrated solution or a ligand vapor.[50] For example, ZIF-8 was exposed to various halogenated imidazoles in the vapor phase.[110] Additionally, defects can be introduced in MOFs through etching using chemicals (such as acids or bases) or plasma treatment.[50,88]

Defects in DE-MOFs can be characterized using various techniques, including topological, structural, and quantitative studies.[35,105–107] Scanning and transmission electron microscopy

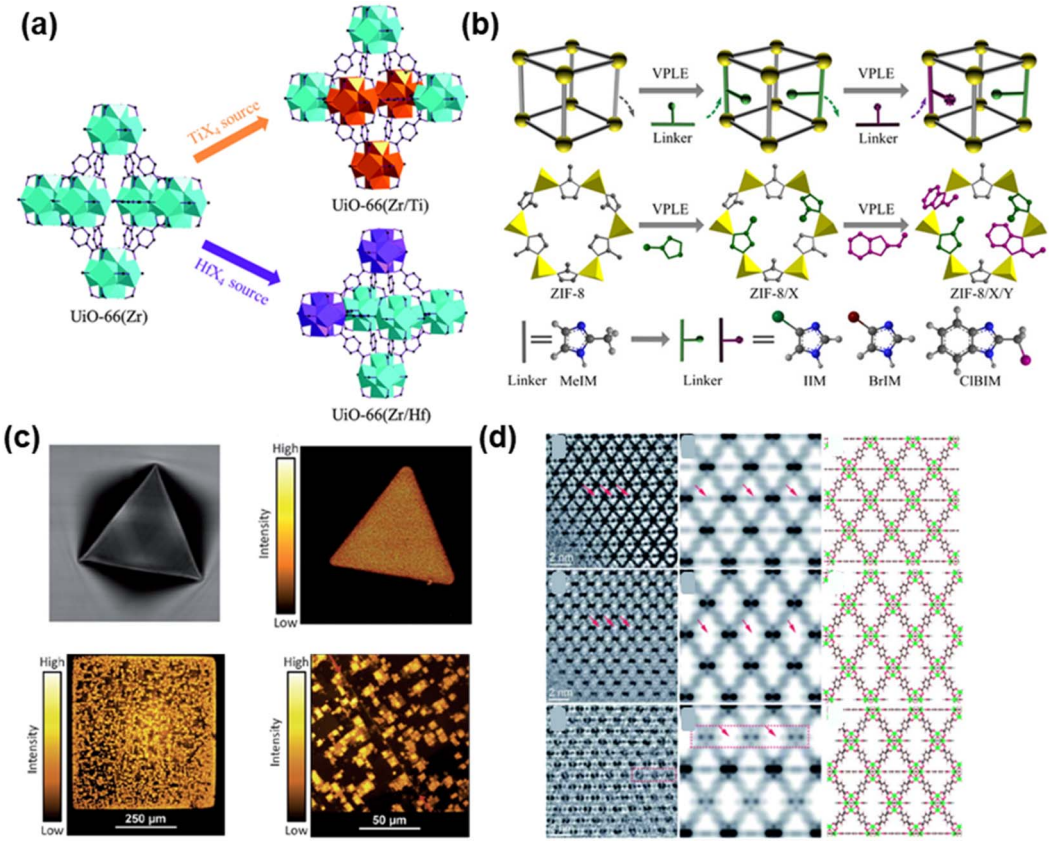

Fig. 8 DE-MOFs. (a) UiO-66 modified with metal exchange.[111,112] Copyright 2016. Reproduced with permission from the Royal Society of Chemistry. (b) ZIF-8 modified by vapor-phase ligand exchange.[110] Copyright 2020. Reproduced with permission from American Association for the Advancement of Science. (c) CFM images showing the defective structures of single crystals of HKUST-1 (top row) and MOF-5 (bottom row);[106] Copyright 2017. Reproduced with permission from Elsevier. (d) HRTEM of MOFs without defects (top row), with missing linker defects (middle row), and with missing cluster defects (bottom row).[107] Copyright 2020. Reproduced with permission from the Royal Society of Chemistry.

Table 3 Materials and CO_2 separation results of TFN and NFN membranes containing various advanced MOFs

		Selective layers							Selectivity			
Membranes	Support/ gutter layer	Polymers	MOFs	Size (nm)	MOF (wt%)	l (nm)	T (°C)/ p (bar)	CO_2 (H_2) permeance (GPU)	CO_2/ N_2	CO_2/ CH_4	H_2/ CO_2	Ref.
NFN	PAN	$Cu(SIF)_6(pyz)_3$@PEG		5–10	80	50	25/1	(3643)			76	114
	Si/ZnO	Pebax	HKUST-1	15	0	100	25/1	(543)			13	115
					—	100		(8460)			41	
TFN	α-Al_2O_3	Pebax 2533	—		—	6000	25/1	150	19			113
			H-UiO-66		6	800		1876	41			
	PES	Pebax	—		—	1870	25/1	150	18			116
			UiO-66	60	2	640		656	50			
	PSF	Pebax	—		—	220	25/1	394	25			117
			ASM-202	78	10	267		936	52			
	AAO		ZIF-62	—	—	2000	25/1	551	28	30		118
	PSF	Pebax	2D ZIF-8	3.5 nm × 1.6 μm	0	—	35/2	161	44			119
					10	780		710	77			
	PAN	6FDA-DAM	NTU-82	5–6	0	600	25/3	250		19		120
					15	800		1190		20		

(SEM and TEM) can be used to monitor changes in MOF topologies. Structural defects can be validated using powder and single-crystal X-ray diffraction (PXRD and SXRD), BET surface area and pore volume, thermogravimetric analysis (TGA), nuclear magnetic resonance (NMR), and positron annihilation lifetime spectroscopy (PALS) (Fig. 8c and d). Various 3D

tools can also be used, such as confocal fluorescence microscopy (CFM), fluorescence lifetime imaging (FLIM), and scanning electron diffraction (SED). X-ray absorption near-edge structure (XANES) and extended X-ray absorption fine structure (EXAFS) have also been used to measure defects quantitatively.[106,107]

DE-MOFs have gained significant interest in designing TFN membranes, as summarized in Table 3. For instance, hollow UiO NPs (H-UiO) were synthesized using an anisotropic acid etching method and then embedded in Pebax-2533 to fabricate membranes for CO_2 separation.[113] The H-UiO NPs were characterized using potentiometric acid–base titration, XRD, BET, and ^{1}H NMR to confirm the crystalline structure and missing linkers. For example, NMR results showed that acid etching decreased the molar ratio of acetate to terephthalate, indicating the presence of missing linkers and an increased content of defect-terminal hydroxyl groups. Adding 6 mass% H-UiO-66 in 6 μm films enhanced CO_2 permeance by 240% from 150 to 520 GPU and CO_2/N_2 selectivity by 130% from 19 to 44. By contrast, adding 6 mass% conventional UiO-66 increased CO_2 permeance only to 380 GPU and CO_2/N_2 selectivity to 34.[113]

Fig. 9a displays a hybrid filler of CNC@UiO-66 with unsaturated metal sites, which interact with CO_2, resulting in increased separation performance.[116] For instance, adding 1 wt% fillers in TFN membranes (Fig. 9b) increased CO_2 permeance from 150 to 644 GPU and CO_2/N_2 selectivity from 18 to 44, surpassing the upper bound (Fig. 9c).

DE-MOFs can also be surface-functionalized to further improve CO_2/N_2 separation properties.[121,122] For instance, defective UiO-66-NH_2 was synthesized by the modulation with trifluoroacetic acid (TFA), which was then modified with an IL, [bmim][Tf_2N].[121] The modification improved their dispersibility and compatibility with PIM-1 and affinity towards CO_2, enhancing CO_2 solubility and CO_2/N_2 solubility selectivity. Similar approaches have been used to improve CO_2 separation properties in MMFs.[123–127]

3.3. TFN membranes based on aMOFs

Compared to conventional MOFs, aMOFs preserve the same connection between the metal nodes and ligands with potential porosity,[128–130] but they have short-range orders, instead of long-range orders, resulting in diffusive peaks instead of sharp peaks in XRD patterns.[129,130] The aMOFs can be obtained from MOFs using several methods, such as pressure-, heat-, and mechanical milling-induced amorphization (Fig. 10a).[39,131–133] Specifically, if a MOF exhibits a melting temperature (T_m) lower than its decomposition temperature (T_d), the MOF can be melted and rapidly cooled to form glassy MOFs (g-MOFs), a sub-category of aMOFs.[38,131]

The aMOFs can be used as fillers for gas separation. For instance, ASM-202 NPs of 80 nm were embedded in Pebax (~250 nm) (Fig. 10b and c);[117] incorporating 10 wt% ASM-202 increased CO_2 permeance from 394 to 936 GPU and CO_2/N_2 selectivity from 25 to 52, which can be partially ascribed to its amorphous structure. Additionally, ASM-202 provided more open metal sites and N-doped structures with affinity towards CO_2.

The g-MOFs attract attention due to their absence of grain boundaries and good filler/polymer compatibility.[48,118,135–142] Notably, g-MOFs can only be obtained from a limited number of MOFs because amorphization usually needs high temperatures above 350–400 °C, while only a few types of ZIFs (like ZIF-4 and

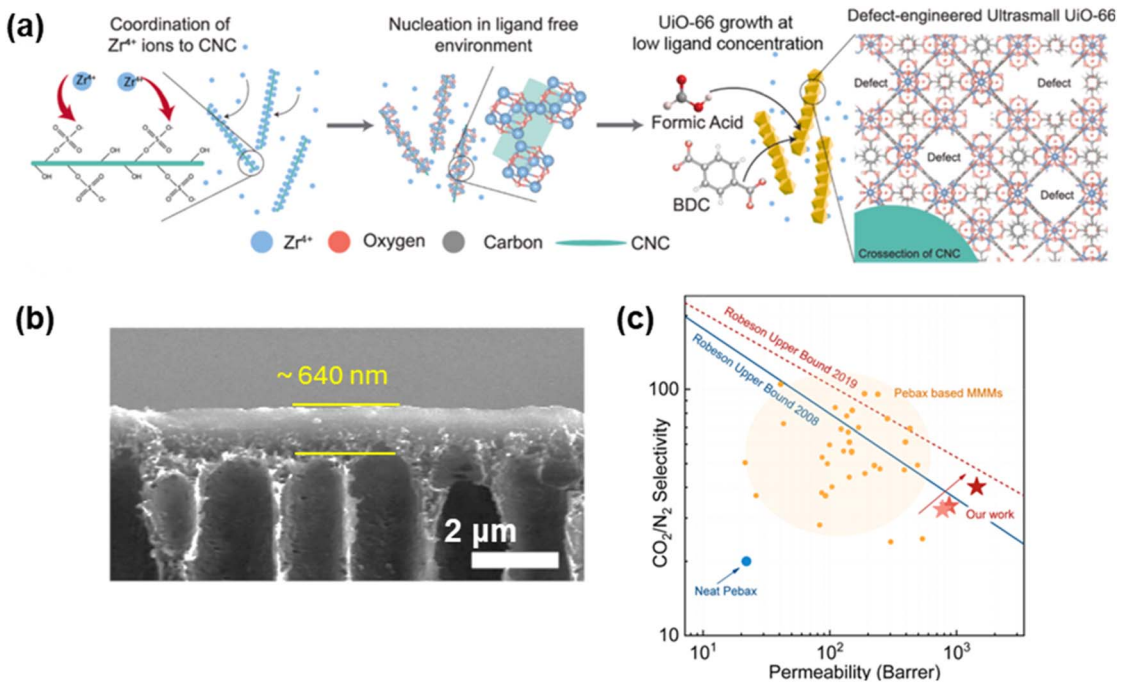

Fig. 9 TFN membranes with DE-MOFs. (a) Synthesis of DE-UiOs by acid modulation, (b) cross-section images of membranes containing 2 wt% DE-UiOs, and (c) gas separation properties.[116] Copyright 2025. Reproduced with permission from Elsevier.

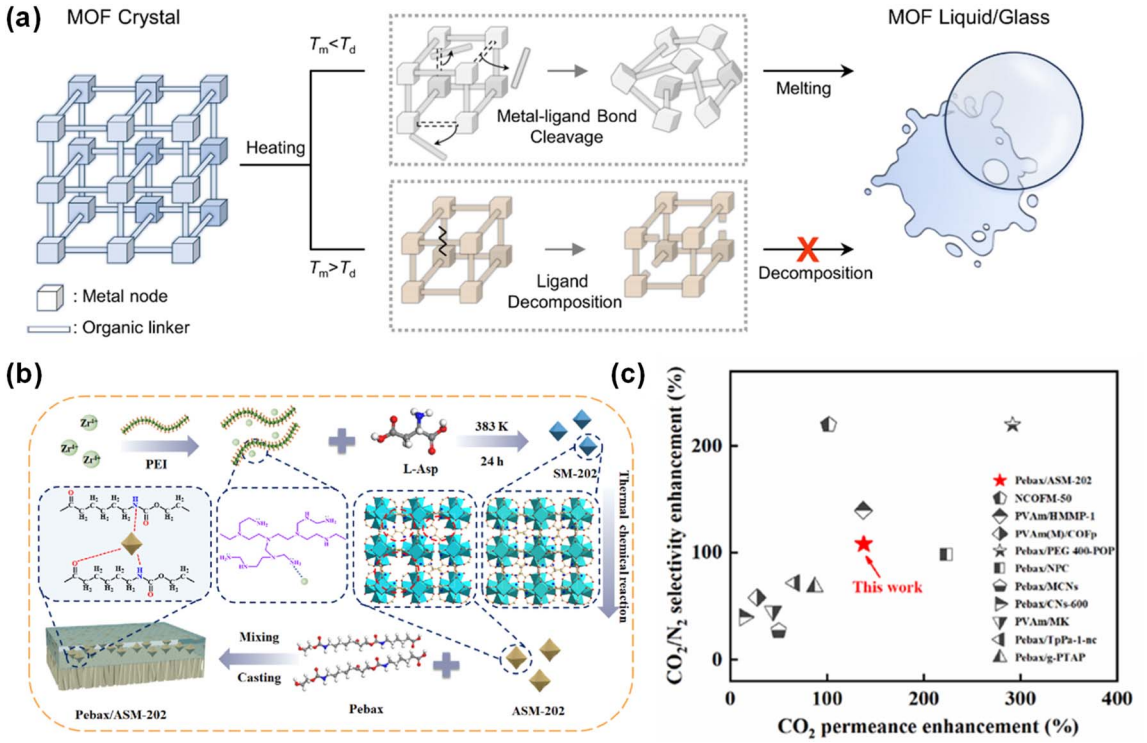

Fig. 10 TFN membranes based on aMOFs. (a) Melt-quenching process to prepare aMOFs from MOFs;[134] Copyright 2024. Reproduced with permission from Springer Nature. (b) Schematic of membranes based on amorphous ASM-202 and (c) enhanced CO_2/N_2 separation properties.[117] Copyright 2024. Reproduced with permission from Elsevier.

ZIF-6) can be stable at such temperatures.[48,142] However, g-MOFs usually exhibit lower porosity than MOFs and therefore lower gas permeability. To address this issue, glassy ZIF-62 (g-ZIF-62) was prepared by *in situ* thermal treatment at 420 °C in PIM-1.[135] The thermal treatment removed interfacial voids of g-ZIF-62/PIM-1 and partially cross-linked the polymer, enhancing the free volume and gas permeability. For instance, introducing 30 wt% g-ZIF-62 increased CO_2 permeability from 4654 to 5914 Barrer and CO_2/CH_4 selectivity from 18 to 66 at 25 °C.

The aMOFs can be blended with conventional MOFs, forming a crystal-glass composite membrane (CGCM).[48,142–146] The MOF has a T_d higher than the T_m of the g-MOF, and thus, its crystalline structure can be preserved during the melting process, while avoiding the formation of voids between the filler and polymer. Additionally, microporous polymers with low melting temperatures (180 °C) were used to prepare CGCMs, instead of g-MOFs.[141] Crystalline MIL-101 NPs with a high surface area were dispersed into the Zn–P-dmbIm (a coordination polymer) with a relatively low surface area. MIL-101 preserved its crystalline structure during the heating process, and adding 10 wt% MIL-101 dramatically increased CO_2 permeability from 850 to 19 000 Barrer and CO_2/N_2 selectivity from 3 to 62.

Glassy ZIF-62 membranes were also prepared using a large-molecule solvent as the structure-directing agent (SDA), resulting in large pores preserved in ZIFs with different topologies.[137] Consequently, the g-MOF NPs exhibited high porosity and formed continuous channels, resulting in CO_2 permeance of 37 000 GPU and good CO_2/N_2 selectivity of 15.[137]

3.4. TFN membranes based on polyMOFs

PolyMOFs have been synthesized using polymers as ligands in the MOFs (Fig. 11a).[40,42,147–149] They combine the crystalline structure of MOFs and the amorphous behavior of polymers. PolyMOFs have been explored for gas separations.[150,151] However, they often had large particles, making them unfavorable for membrane applications.

To address this issue, polyMOFs were synthesized by *in situ* growth of UiO-66 with cPIM-1 with functional moieties similar to the ligand (Fig. 11b).[150] Increasing the cPIM-1 content decreased the crystallinity, ultramicropore size, and CO_2-sorption-derived surface area but decreased microporosity and N_2-sorption-derived surface area, which was beneficial for CO_2/N_2 separation. The obtained polyMOF NPs exhibited good dispersibility in coating solutions and were then added to PIM-1 with good compatibility. TFC membranes with a selective layer (~3 μm) containing 20 wt% polyMOFs were fabricated at a large scale (9–400 cm^2), and they exhibited CO_2 permeance of 4800 GPU and CO_2/N_2 selectivity of 21 (Fig. 11c and d).

3.5. TFN membranes based on MC-MOFs

MC-MOFs were developed by incorporating macrocycle molecules in the frameworks, including crown ethers (CEs), cyclodextrins, calixarenes, and pillararenes (Fig. 12a).[43,44,152] Due to their limited rotational degrees, these macrocyclic hosts possess well-defined cavities for functionalization. As such, MC-MOFs exhibit crystalline structure, high surface area, and functional cavities.[44]

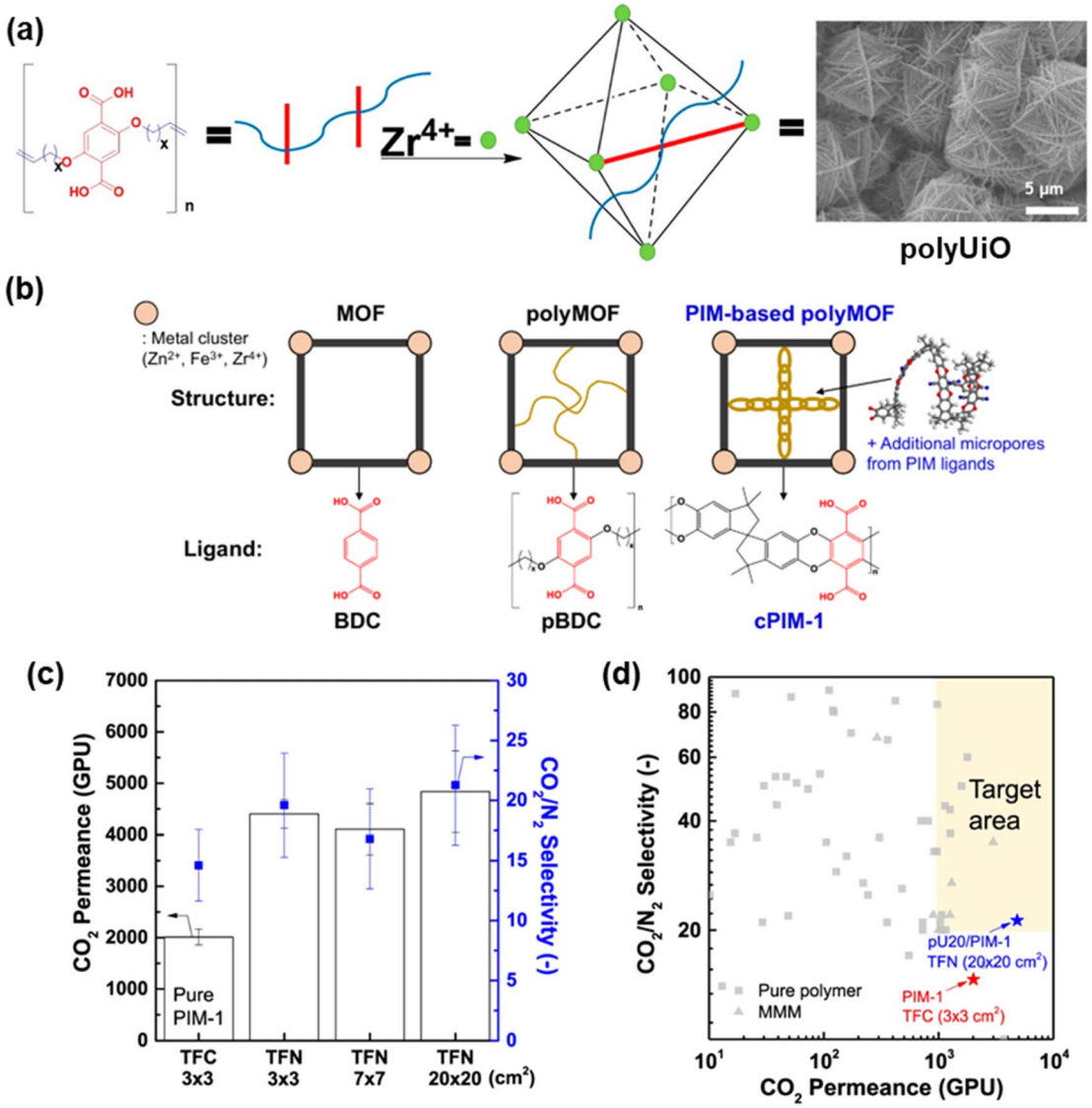

Fig. 11 TFN membranes based on polyMOFs. (a) Schematic of synthesis and SEM image of polyUiO.[40] Copyright 2020. Reproduced with permission from American Chemical Society. (b) Synthesis of MOF, polyMOFs, and cPIM-based polyMOFs,[150] (c) CO_2/N_2 separation properties, and (d) comparison with the leading membranes.[150] Copyright 2023. Reproduced with permission from Springer Nature.

Macrocycles can be incorporated in MOFs using covalent grafting to the surface and non-covalent blending for pore tuning, and they may be directly used as a ligand in synthesizing MOFs.[44] For instance, CEs can be trapped inside the frameworks during the MOF synthesis.[153] Additionally, carboxylic- and nitrobenzo-functionalized CEs were used to modify the MOF surface, which increased dispersibility and separation performance.[154,155] Notably, due to steric hindrance, macrocycles tend to exhibit low reactivity for functionalization.[44]

Fig. 12b shows that MOFs were surface-modified using CEs to enhance dispersibility and stability within the polymers.[155] CEs have cyclic cavities, which are hydrophobic inside and hydrophilic outside, and they have been investigated for ion separations. Specifically, carboxylic-based 21-Crown-7-Ether (21CE-COOH) was used to modify the exterior surface of a series of MOFs with a coordination bond between the –COOH group of CE and metal ions. The surface modification enhanced MOF-solvent interaction and prevented inter-particle agglomeration, improving dispersibility in the polymer. CE-MOFs were also incorporated in polyimides (Fig. 11c); adding CE-functionalized MOFs increased CO_2 adsorption capacity to 1.75×10^{-2} mmol g^{-1} (resulting in CO_2/N_2 selectivity of 70), while adding MOF and a mixture of MOF and CE achieved CO_2 adsorption capacity of 0.75×10^{-2} and 1.0×10^{-2} mmol g^{-1}, respectively.

Nitrobenzo-based CE was used to modify the surface of Azo-UiO-66 NPs, enhancing their compatibility with Pebax-1657 and increasing SO_2/N_2 selectivity from 486 to 643.[154] Additionally, CEs were encapsulated in the dynamic cage of ZIF-7, narrowing the pore size and increasing N_2/CH_4 selectivity from 2 to 7.[156]

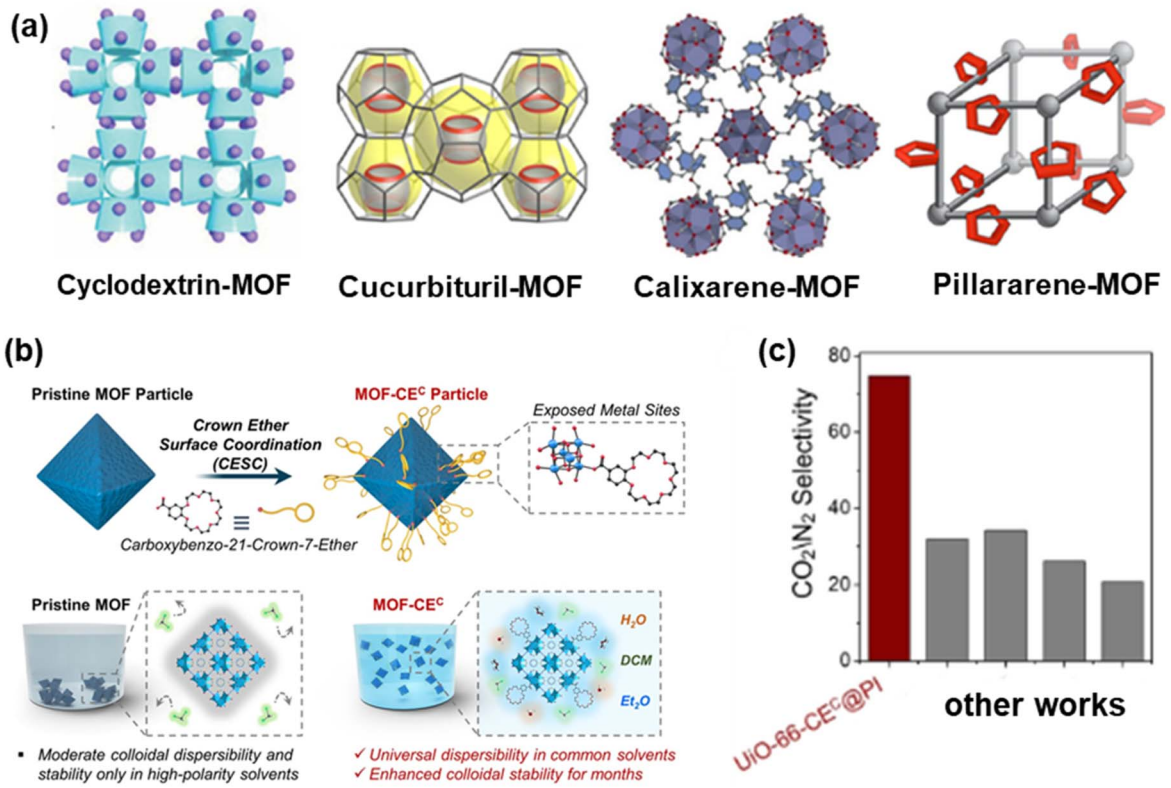

Fig. 12 TFN membranes based on MC-MOFs. (a) Example of MC-MOFs.[44] Copyright 2025. Reproduced with permission from Elsevier. (b) Scheme of surface modification of MOFs with carboxylic CEs and (c) separation performance;[155] Copyright 2023. Reproduced with permission from John Wiley & Sons, Inc.

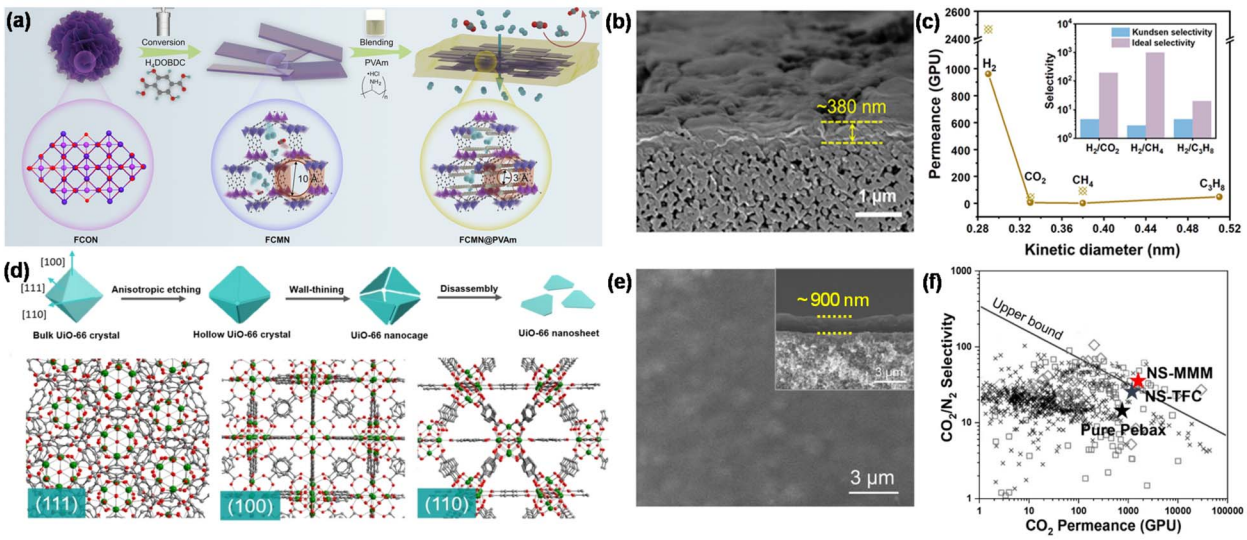

Fig. 13 TFN membranes based on 2D MOFs. (a) Preparation of bi-metallic MOF-74; (b) cross-section view, and (c) superior H_2/CO_2 separation properties.[160] Copyright 2024. Reproduced with permission from Elsevier. (d) Preparation of UiO nanosheets by etching, (e) cross-section image, and (f) superior CO_2/N_2 separation performance.[161] Copyright 2023. Reproduced with permission from John Wiley & Sons, Inc.

3.6. TFN membranes based on 2D MOFs

TFN membranes using ultrathin 2D nanosheet MOFs have been explored for CO_2 separations,[119,120,157–160] because 2D MOFs with high aspect ratios provide better interactions/interfaces with polymers, mitigating interfacial voids.[120] For example, bimetallic MOF-74 nanosheets with open metal sites were synthesized (Fig. 13a) and blended with PVAm and fabricated into TFN membranes with a 300 nm selective layer (Fig. 13b); the membrane exhibited an outstanding H_2 permeance of 1000 GPU and H_2/CO_2

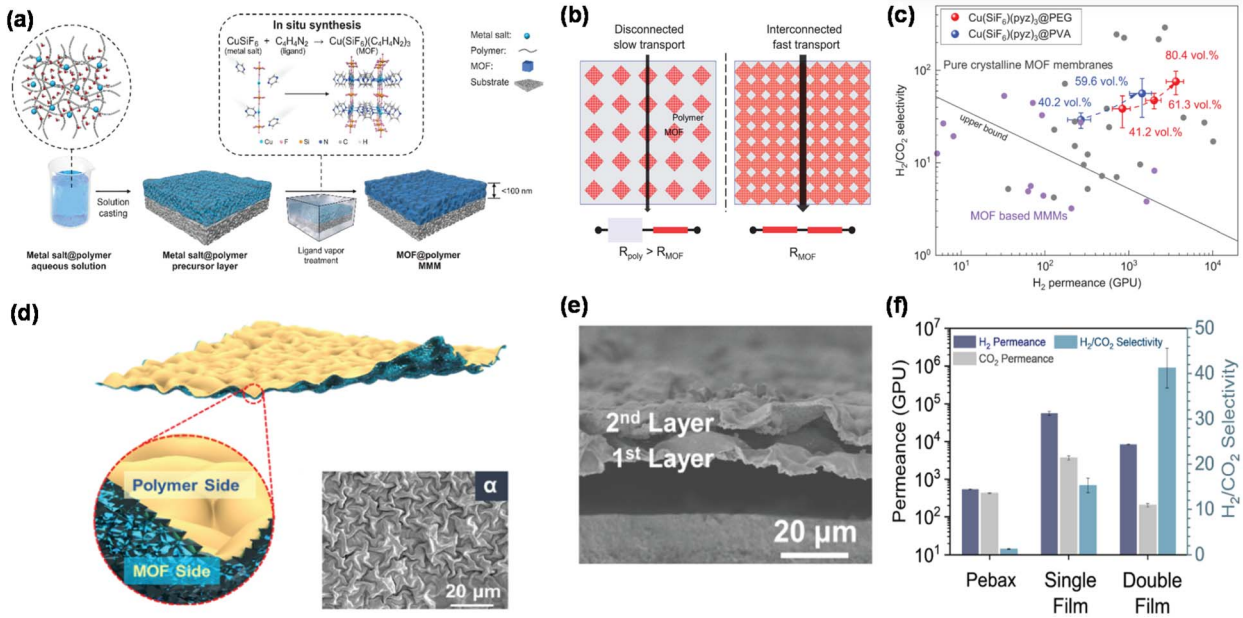

Fig. 14 TFN membranes based on other engineered MOFs. (a) Schematic of membranes comprising 80 vol% MOFs in the polymer, (b) interconnected pathways, and (c) superior H_2/CO_2 separation properties.[114] Copyright 2023. Reproduced with permission from the American Association for the Advancement of Science. (d) Scheme of double-sided wrinkled TFN membranes (inset shows the α pattern of the membrane), (e) cross-section view, and (f) gas separation performance of Pebax, single, and double wrinkled films.[45] Copyright 2023. Reproduced with permission from the American Association for the Advancement of Science.

selectivity of 800, far exceeding Robeson's upper bound (Fig. 12c).[160]

UiO nanosheets were also synthesized from bulk crystals using an anisotropic etching method (Fig. 13d), and they were fabricated into Pebax-based TFN membranes with the selective layer of 900 nm (Fig. 13e);[161] adding 4 wt% nanosheets increased CO_2 permeance by 86% from 747 to 1650 GPU and CO_2/N_2 selectivity by 105% from 16 to 33 (Fig. 13f).

NTU-82 nanosheets containing Hf^{4+} metal cluster were synthesized using a capping agent (formic acid), leading to H-bonds between the nanosheets with 6FDA-DAM and PIM-1.[120] Adding 15 mass% nanosheets in the 6FDA-DAM selective layer (800 nm) increased CO_2 permeance from 250 to 1190 GPU while retaining CO_2/N_2 selectivity of 20, while adding 15 mass% nanosheets in PIM-1 (1500 nm) increased CO_2 permeance from 480 to 2520 GPU while retaining CO_2/N_2 selectivity of ≈13.

3.7. TFN membranes based on other engineered MOFs

Advanced MOFs with unique morphologies have been made, such as interconnected channels, wrinkled surfaces, and interwoven networks. Fig. 14a illustrates a solid-solvent processing method to prepare a nanolayer of TFN membranes

Table 4 Various strategies for engineering MOFs and their respective pros and cons

MOFs	Synthesis mechanism	Procedures	Effects on gas separation properties
Conventional MOFs	Mixing metal clusters and organic ligands in a solvent	Coordination bonds between metal and ligand	Temperature, modulating agent, and solvent affect NP sizes and morphologies
SM-MOFs	Modifying the surface of MOFs with coordination or covalent bonds	Using chemicals after MOF formation	Enhanced polymer-MOF compatibility and functionalities
DE-MOFs	Adjusting metal–ligand coordination bonds	Mixed ligands or metal ions, or post-exchange with ligands or metal ions	Missing linkers or metal centers; increased porosity and surface area
aMOFs	Transition from crystalline to amorphous MOFs	Melt-quenching; pressure and mechanical milling	Mitigated grain boundaries and filler-polymer interfacial voids
polyMOFs	Interaction between metal centers and ligand-like polymers	Adding polymeric co-ligands to the parent solutions	Enhanced MOF dispersibility and functionalities
MC-MOFs	Coordination with open metal centers on MOF surface	Using macrocycles as the co-ligands or surface-modifying agents	Creating additional selective gates and enhancing MOF dispersibility
2D MOFs	Top-down or bottom-up approaches	Stacking MOF layers along the vertical direction *via* weak interaction forces	Enlarged surface area; enhanced open metal sites; shorter transport pathway

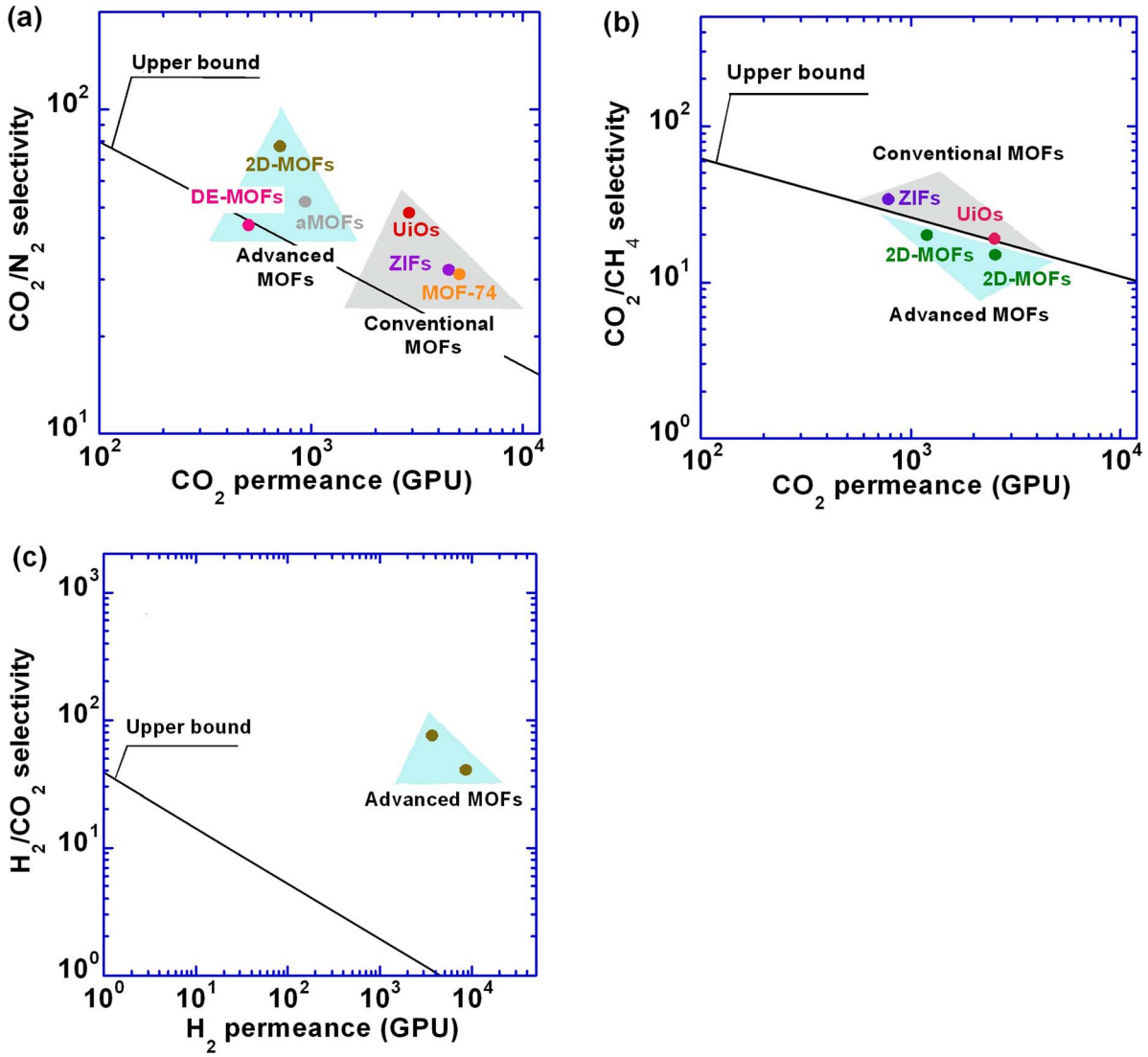

Fig. 15 TFN membranes comprising conventional and advanced MOFs for (a) CO_2/N_2 separation, (b) CO_2/CH_4 separation, and (c) H_2/CO_2 separation. The upper bounds were drawn assuming a selective layer thickness of 1 μm.

containing 80 vol% MOFs.[114] The MOFs were dispersed at a molecular level in the polymer because the polymer can dissolve the metal salt. The selective layer had a filler-dominant structure with interconnected channels for gas transport (Fig. 14b), resulting in high separation performance (Fig. 14c).

Wrinkled MOF films with various Turing (wrinkled) patterns were synthesized by changing the reagent concentrations before coating with a Pebax layer (Fig. 14d).[45] The obtained membranes exhibited H_2 permanence of 8460 GPU and H_2/CO_2 of 41 (Fig. 14e and f).

Interwoven MOF-gel polymer networks were also used to prepare NFN membranes with selective layers as thin as 50 nm.[162] Their molecular weaving strategy resulted in flexible 3D UiO-66 gel networks incorporating PEI and GA, which provided H-bonding and coordination with MOF gels. The obtained membranes achieved H_2 permanence of 845 GPU and H_2/CO_2 selectivity of 17, and their fabrication was successfully scaled up to a large area (>160 cm^2).

4. Discussions

4.1. Comparison of MOFs for their improvement in separation properties

Table 4 summarizes the formation mechanisms, structure characteristics, and enhancement in gas separation for conventional and engineered MOFs. Each engineered MOF represents an effective way to enhance membrane separation properties, and its effects depend on its unique structure and interactions with the polymer matrix.

Fig. 15 and Table 5 highlight the use of advanced MOFs to enhance the separation properties of CO_2/N_2, CO_2/CH_4, and H_2/CO_2. The enhancement of gas permeance and selectivity by adding MOFs can also be characterized by permeance enhancement (β_P, %) and selectivity enhancement (β_S, %), which are defined as the increase relative to those of the pristine polymeric membranes. Furthermore, the overall enhancement

Table 5 Materials and CO_2 separation results of TFN and NFN membranes containing conventional and engineered MOFs

Separations	Category	Samples	β_P (%)	β_S (%)	F_{index} (%)	Ref.
CO_2/N_2	MOFs	*a*PEO + UiO	107	−4	0.61	165
		POEM + ZIF	312	−20	0.77	76
		PIM + MOF-74	16	63	1.6	74
	Engineered MOFs	Pebax + DE-MOFs	265	132	3.7	113
		Pebax + aMOFs	137	108	3.0	117
		Pebax + 2D MOF	341	75	3.1	119
CO_2/CH_4	MOFs	PI + ZIF	156	55	2.1	101
		PIM + UiO	−45	46	0.39	85
	Engineered MOFs	6FDA-DAM + 2D	376	5	1.7	120
		PIM + 2D MOF	425	25	2.3	
H_2/CO_2	Engineered MOFs	$Cu(SIF)_6(pyz)_3$@PEG	—	—	—	114
		Pebax + HKUST	1460	215	5.4	115

in the separation performance is given by a filler enhancement index (F_{index}):[163]

$$F_{index} = \ln\left(\frac{Q_M}{Q_P}\right) + \lambda_{A/B}\ln\left(\frac{\alpha_M}{\alpha_P}\right) = \ln(\beta_P + 1) + \lambda_{A/B}\ln(\beta_S + 1) \quad (10)$$

where $\lambda_{A/B}$ is the slope of the upper bound, and it has a value of 2.888, 2.636, and 2.302 for CO_2/N_2, CO_2/CH_4, and H_2/CO_2 separation, respectively.[164] Fig. 15 shows that incorporating the advanced MOFs in the TFN membranes overcomes the permeance and selectivity tradeoff, surpassing Robeson's upper bounds.

4.2. Scale-up of TFN membranes

Though rarely, large-scale TFN membranes have been successfully produced. For example, NFN membranes based on interwoven MOF-gel polymer networks (50 nm) were prepared at 160 cm^2 using a blade casting technique;[162] membranes based on cPIM-1 and polyUiO (~3 μm) were fabricated at 400 cm^2 using a scalable bar-coating method;[150] membranes based on *a*PEO and UiO-66-NH_2 were fabricated at ~100 cm^2 using an automatic coating machine;[52] membranes based on PVAm and rigid ZIF-8 were fabricated at 3100 cm^2 with a blade casting method.[166] Notably, NFN membranes with MOF layers of 50–130 nm were also successfully synthesized at 2400 cm^2 for gas separations.[167,168] Nevertheless, we envision that if MOF NPs can be dispersed in polymer coating solutions, TFN membranes can be fabricated using the roll-to-roll process developed for polymeric membranes.

5. Conclusion and perspectives

The platform of TFN membranes represents a fruitful marriage of polymeric membranes and MOFs with an enormous library of chemistry, pore size, porosity, and morphology. Many membranes present CO_2 separation properties above Robeson's upper bound and surpassing state-of-the-art polymeric membranes. We expect that TFN and NFN membranes will continue to make great strides in the coming decades, and the following challenges should be addressed to bring this exciting materials platform to practical use. First, more studies should focus on the scalable fabrication of TFN membranes consistently using roll-to-roll processes (as opposed to thick free-standing films), similar to the challenges faced by many nanomaterials for practical applications.[169] The aggregation and distribution of the MOFs in thin films should be controlled to optimize gas separation properties. For example, the location of the NPs on the surface or at the bottom of the selective layers exerts a dramatic influence on gas permeance.

Second, there is an imperative need to understand the difference between the bulk films and nanofilms for nanocomposites, which is critical to designing NFN membranes.[85,170,171] The polymer chain dynamics of the nanofilms can be influenced by their thickness, particularly in the presence of MOF NPs with diameters comparable to the selective layer thickness, which affects polymer chain conformations and packing density in the particle/polymer interface, impacting molecular separation properties.[170] For instance, decreasing the thickness from 60 μm to 35 nm dramatically decreased gas permeability for 6FDA-DAM (by 72%) and PIM-1 (by 87%) due to the nanoconfinement-induced microstructure change and physical aging.[172] Despite a rich literature focusing on polymer dynamics of nanocomposites containing NPs (like silica and Au),[173] there are very few studies on MOF-based TFNs. Additionally, the nano-confinement in the thin films may also influence the NP aggregation and distribution.

Third, while the pore sizes and porosity of MOFs have been extensively explored to improve gas diffusivity and selectivity, the potential affinity between the MOFs and targeted gases has been rarely investigated.[174] Particularly, MOFs can have open metal sites (OMS), such as MOF-74 and HKUST-1, which have high metal site density and strong interactions with various gas molecules.[175,176] We also expect that new MOFs can be designed with modeling, simulation, and machine learning for membrane gas separations,[177–179] similar to other scientific fields that have been involved in and developed through the use of artificial intelligence (AI).[180–182]

Finally, for MOFs to be incorporated into nanofilms of <100 nm in NFN membranes, they should be less than 100 nm in diameter and preferably less than 50 nm. Therefore, it is crucial to be able to synthesize nano-sized MOFs with high yields on a large scale at a low cost.

Conflicts of interest

The authors declare no competing financial interests.

Data availability

Data are available upon request to the corresponding author.

Acknowledgements

This work received financial support from the U.S. Department of Energy Small Business Technology Transfer Program (DE-SC0020730).

References

1 W. J. Koros and C. Zhang, *Nat. Mater.*, 2017, **16**, 289–297.
2 M. Galizia, W. S. Chi, Z. P. Smith, T. C. Merkel, R. W. Baker and B. D. Freeman, *Macromolecules*, 2017, **50**, 7809–7843.
3 M. Sanderu, E. M. Sandru, W. F. Ingram, J. Deng, P. M. Stenstad, L. Deng and R. J. Spontak, *Science*, 2022, **376**, 90–94.
4 Y. Han and W. Ho, *J. Membr. Sci.*, 2021, **628**, 119244.
5 H. Park, J. Kamcev, L. M. Robeson, M. Elimelech and B. D. Freeman, *Science*, 2017, **356**, eaab0530.
6 Y. Hua, S. Park and H.-K. Jeong, *J. Environ. Chem. Eng.*, 2024, **12**, 113753.
7 L. Hu, K. Chen, W. I. Lee, K. Kisslinger, C. Rumsey, S. Fan, V. T. Bui, N. Esmaeili, T. Tran, Y. Ding, M. Trebbin, C.-Y. Nam, M. T. Swihart and H. Lin, *Adv. Mater.*, 2023, **35**, 2301007.
8 M. S. Denny, J. C. Moreton, L. Benz and S. M. Cohen, *Nat. Rev. Mater.*, 2016, **1**, 1–17.
9 G. Cai, P. Yan, L. Zhang, H. Zhou and H. Jiang, *Chem. Rev.*, 2021, **121**, 12278–12326.
10 Q. Qian, P. A. Asinger, M. J. Lee, G. Han, K. Mizrahi Rodriguez, S. Lin, F. M. Benedetti, A. X. Wu, W. S. Chi and Z. P. Smith, *Chem. Rev.*, 2020, **120**, 8161–8266.
11 Q. Zhao, S. Lian, R. Li, Z. Yu, Q. Liu, G.-L. Zang and C. Song, *Chem. Eng. J.*, 2022, **443**, 136290.
12 K.-G. Liu, F. Bigdeli, A. Panjehpour, S. Hwa Jhung, H. A. J. Al Lawati and A. Morsali, *Coord. Chem. Rev.*, 2023, **496**, 215413.
13 L. Hu, K. Clark, T. Alebrahim and H. Lin, *J. Membr. Sci.*, 2022, **644**, 120140.
14 M. Liu, M. D. Nothling, P. A. Webley, Q. Fu and G. G. Qiao, *Acc. Chem. Res.*, 2019, **52**, 1905–1914.
15 D. Zhao, F. Feng, L. Shen, Z. Huang, Q. Zhao, H. Lin and T.-S. Chung, *Chem. Eng. J.*, 2023, **454**, 140447.
16 Y. Duan, L. Li, Z. Shen, J. Cheng and K. He, *Membranes*, 2023, **13**, 1–31.
17 Y. Jia, K. Wong, C. Z. Liang, J. Wu, T.-S. Chung and S. Zhang, *Prog. Mater. Sci.*, 2024, **146**, 101324.
18 Z. Yang, P. F. Sun, X. Li, B. Gan, L. Wang, X. Song, H. D. Park and C. Y. Tang, *Environ. Sci. Technol.*, 2020, **54**, 15563–15583.
19 G. Zhang and H. Lin, *Green Energy Environ.*, 2024, **9**, 1220–1238.
20 J. Wu, F. Hillman, C.-Z. Liang, Y. Jia and S. Zhang, *J. Mater. Chem. A*, 2023, **11**, 17452–17478.
21 F. Pazani, M. Shariatifar, M. Salehi Maleh, T. Alebrahim and H. Lin, *Sep. Purif. Technol.*, 2023, **308**, 122876.
22 Z. Dai, J. Deng, L. Ansaloni, S. Janakiram and L. Deng, *J. Membr. Sci.*, 2019, **578**, 61–68.
23 A. Raza, M. Askari, C. Z. Liang, N. Peng, S. Farrukh, A. Hussain and T.-S. Chung, *J. Membr. Sci.*, 2021, **625**, 119124.
24 Y. Cheng, S. J. Datta, S. Zhou, J. Jia, O. Shekhah and M. Eddaoudi, *Chem. Soc. Rev.*, 2022, **51**, 8300–8350.
25 M. R. A. Hamid, Y. Qian, R. Wei, Z. Li, Y. Pan, Z. Lai and H.-K. Jeong, *J. Membr. Sci.*, 2021, **640**, 119802.
26 W. Su, Y. Xiang, Y. Dai, Y. Wang, S. Zhong and J. Li, *Chem. Commun.*, 2024, **60**, 7124–7135.
27 B. Ghalei, K. Sakurai, Y. Kinoshita, K. Wakimoto, A. P. Isfahani, Q. Song, K. Doitomi, S. Furukawa, H. Hirao and H. Kusuda, *Nat. Energy*, 2017, **2**, 1–9.
28 N. Tien-Binh, D. Rodrigue and S. Kaliaguine, *J. Membr. Sci.*, 2018, **548**, 429–438.
29 Y. Song, S. Zheng, Y. Ji, B. He and M. Wang, *Chem. Eng. J.*, 2025, **518**, 164526.
30 M. Zeeshan, H. C. Gulbalkan, O. Durak, Z. P. Haslak, U. Unal, S. Keskin and A. Uzun, *Adv. Funct. Mater.*, 2022, **32**, 2204149.
31 S. Hussain, A. Ali, S. Foorginezhad, Y. Chen and X. Ji, *Sep. Purif. Technol.*, 2024, **360**, 130997.
32 L. Zhang, Y. He and Y. Fu, *Chem. Commun.*, 2025, **61**, 2878–2890.
33 S. Yu, C. Li, S. Zhao, M. Chai, J. Hou and R. Lin, *Nanoscale*, 2024, **16**, 7716–7733.
34 M. Taddei, *Coord. Chem. Rev.*, 2017, **343**, 1–24.
35 S. Li, W. Han, Q. F. An, K. T. Yong and M. J. Yin, *Adv. Funct. Mater.*, 2023, **33**, 2303447.
36 X. Qiu and R. Wang, *Coord. Chem. Rev.*, 2025, **526**, 216356.
37 M. Kim, Y. Lee and H. R. Moon, *Acc. Chem. Res.*, 2024, **57**, 2347–2357.
38 T. D. Bennett and S. Horike, *Nat. Rev. Mater.*, 2018, **3**, 431–440.
39 Z. Yu, L. Tang, N. Ma, S. Horike and W. Chen, *Coord. Chem. Rev.*, 2022, **469**, 214646.
40 M. Kalaj, K. C. Bentz, S. Ayala Jr, J. M. Palomba, K. S. Barcus, Y. Katayama and S. M. Cohen, *Chem. Rev.*, 2020, **120**, 8267–8302.
41 T. Kitao, Y. Zhang, S. Kitagawa, B. Wang and T. Uemura, *Chem. Soc. Rev.*, 2017, **46**, 3108–3133.
42 S. Kumar, B. Mohan, B. Musikavanhu, X. Wang, R. Muhammad, X. Yang and P. Ren, *Coord. Chem. Rev.*, 2025, **524**, 216286.
43 Y. Liang, E. Li, K. Wang, Z. Guan, H. He, L. Zhang, H. Zhou, F. Huang and Y. Fang, *Chem. Soc. Rev.*, 2022, **51**, 8378–8405.
44 S. Cheng, Y. Liu and Y. Sun, *Coord. Chem. Rev.*, 2025, **534**, 216559.
45 X. Luo, M. Zhang, Y. Hu, Y. Xu, H. Zhou, Z. Xu, Y. Hao, S. Chen, S. Chen and Y. Luo, *Science*, 2024, **385**, 647–651.

46 M. Shan, X. Geng, I. Imaz, A. Broto-Ribas, B. Ortín-Rubio, D. Maspoch, L. Ansaloni, T. A. Peters, A. Tena and M. E. Boerrigter, *J. Membr. Sci.*, 2024, **691**, 122258.
47 Q. Wu, X. He, C. Cui, B. Qi and J. Wei, *Sep. Purif. Technol.*, 2025, **354**, 128946.
48 Y. Zhang, B. H. Yin, L. Huang, L. Ding, S. Lei, S. G. Telfer, J. Caro and H. Wang, *Prog. Mater. Sci.*, 2025, **151**, 101432.
49 S. Sun, Y. Zhang, M. Wang, Y. Zhao, J. Peng, S. Cong and H. Pang, *Ind. Eng. Chem. Res.*, 2025, **64**, 14771–14788.
50 T. Chen and D. Zhao, *Coord. Chem. Rev.*, 2023, **491**, 215259.
51 Q. Ma, J. Li, Y. Li and J. Choi, *J. Membr. Sci.*, 2024, **690**, 122201.
52 G. Zhang, C. J. Shah, W. I. Lee, K. Kisslinger, N. Esmaeili, V. T. Bui, L. Zhu, C. Y. Nam and H. Lin, *Adv. Funct. Mater.*, 2024, **34**, 2404785.
53 T. Alebrahim, L. Huang, H. K. Welgama, N. Esmaeili, E. Deng, S. Cheng, D. Acharya, C. M. Doherty, A. J. Hill, C. Rumsey, M. Trebbin, T. R. Cook and H. Lin, *ACS Appl. Mater. Interfaces*, 2024, **16**, 11116–11124.
54 C. Liang, T.-S. Chung and J.-Y. Lai, *Prog. Polym. Sci.*, 2019, **97**, 101141.
55 M. Yu, A. B. Foster, S. E. Kentish, C. A. Scholes and P. M. Budd, *J. Membr. Sci.*, 2025, **722**, 123844.
56 J. Zhao, G. He, G. Liu, F. Pan, H. Wu, W. Jin and Z. Jiang, *Prog. Polym. Sci.*, 2018, **80**, 125–152.
57 L. Zhu, M. Yavari, W. Jia, E. P. Furlani and H. Lin, *Ind. Eng. Chem. Res.*, 2017, **56**, 351–358.
58 M. Kattula, K. Ponnuru, L. Zhu, W. Jia, H. Lin and E. P. Furlani, *Sci. Rep.*, 2015, **5**, 15016.
59 M. Liu, K. Xie, M. D. Nothling, P. A. Gurr, S. S. L. Tan, Q. Fu, P. A. Webley and G. G. Qiao, *ACS Nano*, 2018, **12**, 11591–11599.
60 Y. Ma, N. Liu, Y. Zhang, Z. Xu, J. Chen, H. Wu and J. Meng, *J. Environ. Chem. Eng.*, 2025, **13**, 116087.
61 Y. Zhang, L. Xu, X. Hu, B. Chen, X. Chen, Q. Li, H. Mao and Z. Zhao, *Chem. Eng. J.*, 2025, **510**, 161702.
62 M. Liu, K. Xie, M. D. Nothling, L. Zu, S. Zhao, D. J. E. Harvie, Q. Fu, P. A. Webley and G. G. Qiao, *ACS Cent. Sci.*, 2021, **7**, 671–680.
63 Z. Dai, L. Ansaloni and L. Deng, *Green Energy Environ.*, 2016, **1**, 102–128.
64 P. Fu, H. Li, J. Gong, Z. Fan, A. T. Smith, K. Shen, T. O. Khalfalla, H. Huang, X. Qian, J. R. McCutcheon and L. Sun, *Prog. Polym. Sci.*, 2022, **126**, 101506.
65 K. Xie, Q. Fu, C. Xu, H. Lu, Q. Zhao, R. Curtain, D. Gu, P. A. Webley and G. G. Qiao, *Energy Environ. Sci.*, 2018, **11**, 544–550.
66 G. Zhao, W. Han, L. Dong, H. Fan, Z. Qu, J. Gu and H. Meng, *Green Energy Environ.*, 2022, **7**, 1143–1160.
67 X. Qian, M. Ostwal, A. Asatekin, G. M. Geise, Z. P. Smith, W. A. Phillip, R. P. Lively and J. R. McCutcheon, *J. Membr. Sci.*, 2022, **645**, 120041.
68 S. K. Elsaidi, M. Ostwal, L. Zhu, A. Sekizkardes, M. H. Mohamed, M. Gipple, J. R. McCutcheon and D. Hopkinson, *RSC Adv.*, 2021, **11**, 25658–25663.
69 C. Ge, M. Sheng, Y. Yuan, F. Shi, Y. Yang, S. Zhao, J. Wang and Z. Wang, *Carbon Capture Sci. Technol.*, 2024, **10**, 100156.
70 M. Kang, H. Min, S. Kim and J. Kim, *J. Membr. Sci.*, 2024, **698**, 122611.
71 N. Li, Z. Wang, M. Wang, M. Gao, H. Wu, S. Zhao and J. Wang, *J. Membr. Sci.*, 2021, **624**, 119095.
72 L. Martínez-Izquierdo, C. Téllez and J. Coronas, *J. Mater. Chem. A*, 2022, **10**, 18822–18833.
73 H. Min, M.-B. Kim, Y.-S. Bae, P. K. Thallapally, J. H. Lee and J. Kim, *Membranes*, 2023, **13**, 287.
74 M. Liu, M. D. Nothling, P. A. Webley, J. Jin, Q. Fu and G. G. Qiao, *Chem. Eng. J.*, 2020, **396**, 125328.
75 H. Min, M. Kang, Y.-S. Bae, R. Blom, C. A. Grande and J. Kim, *J. Membr. Sci.*, 2023, **669**, 121295.
76 C. Lee, M. Kang, K. Kim and J. Kim, *J. Membr. Sci.*, 2022, **642**, 119913.
77 M. Kang, T. Kim, H. Han, H. Min, Y. Bae and J. Kim, *J. Membr. Sci.*, 2022, **659**, 120788.
78 D. Jiang, C. Huang, J. Zhu, P. Wang, Z. Liu and D. Fang, *Coord. Chem. Rev.*, 2021, **444**, 214064.
79 S. Yuan, L. Feng, K. Wang, J. Pang, M. Bosch, C. Lollar, Y. Sun, J. Qin, X. Yang, P. Zhang, Q. Wang, L. Zou, Y. Zhang, L. Zhang, Y. Fang, J. Li and H. Zhou, *Adv. Mater.*, 2018, **30**, 1704303.
80 A. Kirchon, L. Feng, H. F. Drake, E. A. Joseph and H. Zhou, *Chem. Soc. Rev.*, 2018, **47**, 8611–8638.
81 Z. Hu, I. Castano, S. Wang, Y. Wang, Y. Peng, Y. Qian, C. Chi, X. Wang and D. Zhao, *Cryst. Growth Des.*, 2016, **16**, 2295–2301.
82 S. Fan, J. Wang, L. Liao, J. Feng, B. Li and S. Zhang, *Chem. Eng. J.*, 2023, **468**, 143645.
83 M.-H. Pham, G.-T. Vuong, F.-G. Fontaine and T.-O. Do, *Cryst. Growth Des.*, 2012, **12**, 3091–3095.
84 B. Qiu, M. Yu, J. M. Luque-Alled, S. Ding, A. B. Foster, P. M. Budd, X. Fan and P. Gorgojo, *Angew. Chem., Int. Ed.*, 2024, **63**, e202316356.
85 G. Chen, H. Zhu, G. Liu, G. Liu and W. Jin, *Angew. Chem., Int. Ed.*, 2025, **64**, e202418649.
86 G. Zhang, V. Bui, Y. Yin, E. H. R. Tsai, C. Y. Nam and H. Lin, *ACS Appl. Mater. Interfaces*, 2023, **15**, 35543–35551.
87 J. Lee, J. Lee, J. Y. Kim and M. Kim, *Chem. Soc. Rev.*, 2023, **52**, 6379–6416.
88 Z. Yin, S. Wan, J. Yang, M. Kurmoo and M.-H. Zeng, *Coord. Chem. Rev.*, 2019, **378**, 500–512.
89 H. Molavi, A. Shojaei and S. A. Mousavi, *J. Mater. Chem. A*, 2018, **6**, 2775–2791.
90 B. J. Yao, L. G. Ding, F. Li, J. T. Li, Q. J. Fu, Y. Ban, A. Guo and Y. B. Dong, *ACS Appl. Mater. Interfaces*, 2017, **9**, 38919–38930.
91 X. Jiang, S. Li, S. He, Y. Bai and L. Shao, *J. Mater. Chem. A*, 2018, **6**, 15064–15073.
92 H. Molavi and A. Shojaei, *ACS Appl. Mater. Interfaces*, 2019, **11**, 9448–9461.
93 Q. Qian, A. X. Wu, W. S. Chi, P. A. Asinger, S. Lin, A. Hypsher and Z. P. Smith, *ACS Appl. Mater. Interfaces*, 2019, **11**, 31257–31269.

94 H. Wang, S. He, X. Qin, C. Li and T. Li, *J. Am. Chem. Soc.*, 2018, **140**, 17203–17210.
95 Y. Zhang, X. Feng, H. Li, Y. Chen, J. Zhao, S. Wang, L. Wang and B. Wang, *Angew. Chem., Int. Ed.*, 2015, **54**, 4259–4263.
96 H. Han, J. M. P. Scofield, P. A. Gurr, P. A. Webley and G. G. Qiao, *Adv. Mater. Interfaces*, 2024, **11**, 2400113.
97 X. Su, L. Bromberg, V. Martis, F. Simeon, A. Huq and T. A. Hatton, *ACS Appl. Mater. Interfaces*, 2017, **9**, 11299–11306.
98 S. Fan, C. Liang, F. Feng, K. Wong, K. Wang, S. Jia, N. Bhuwania, S. Zhang and S. Zhang, *Angew. Chem., Int. Ed.*, 2025, **64**, e202421028.
99 S. Min, M. Kang, Y.-J. Jeon, E.-Y. Kim, J. H. Kim and J.-H. Kim, *J. Mater. Chem. A*, 2025, 27356–27366.
100 L. Martínez-Izquierdo, C. García-Comas, S. Dai, M. Navarro, A. Tissot, C. Serre, C. Téllez and J. Coronas, *ACS Appl. Mater. Interfaces*, 2024, **16**, 4024–4034.
101 S. Song, M. Zhao, Z. Guo, Y. Ren, J. Wang, X. Liang, Y. Pu, S. Wang, H. Ma and X. Wang, *J. Membr. Sci.*, 2023, **669**, 121340.
102 S. Dissegna, K. Epp, W. R. Heinz, G. Kieslich and R. A. Fischer, *Adv. Mater.*, 2018, **30**, e1704501.
103 D. Fan, A. Ozcan, O. Shekhah, R. Semino, M. Eddaoudi and G. Maurin, *J. Membr. Sci. Lett.*, 2022, **2**, 100029.
104 Z. Fang, B. Bueken, D. E. De Vos and R. A. Fischer, *Angew. Chem., Int. Ed.*, 2015, **54**, 7234–7254.
105 G. Choi, M. Mandal, H. Jung, J. Panda, Y. Kwon, K. Zhang, E. Vivek, M. Shon, K. Ravi, K. Baek, H. Kwon, J. Yeo and K. Cho, *J. Mater. Sci. Technol.*, 2024, **201**, 95–118.
106 J. Ren, M. Ledwaba, N. M. Musyoka, H. W. Langmi, M. Mathe, S. Liao and W. Pang, *Coord. Chem. Rev.*, 2017, **349**, 169–197.
107 W. Xiang, Y. Zhang, Y. Chen, C.-j. Liu and X. Tu, *J. Mater. Chem. A*, 2020, **8**, 21526–21546.
108 X. Song, T. K. Kim, H. Kim, D. Kim, S. Jeong, H. R. Moon and M. S. Lah, *Chem. Mater.*, 2012, **24**, 3065–3073.
109 D. Sun, W. Liu, M. Qiu, Y. Zhang and Z. Li, *Chem. Commun.*, 2015, **51**, 2056–2059.
110 W. Wu, J. Su, M. Jia, Z. Li, G. Liu and W. Li, *Sci. Adv.*, 2020, **6**, eaax7270.
111 Y. Bai, Y. Dou, L. Xie, W. Rutledge, J. Li and H. Zhou, *Chem. Soc. Rev.*, 2016, **45**, 2327–2367.
112 M. Kim, J. F. Cahill, H. Fei, K. A. Prather and S. M. Cohen, *J. Am. Chem. Soc.*, 2012, **134**, 18082–18088.
113 J. Yan, Y. Sun, T. Ji, M. Wu, S. Meng, W. Dong, Y. Liu, K. Yu, W. Hu, B. Sun, P. Lu, Y. Li, H. Hu and Y. Liu, *AIChE J.*, 2024, **70**, 1–11.
114 G. Chen, C. Chen, Y. Guo, Z. Chu, Y. Pan, G. Liu, G. Liu, Y. Han, W. Jin and N. Xu, *Science*, 2023, **381**, 1350–1356.
115 C. Jiao, X. Song, X. Zhang, L. Sun and H. Jiang, *ACS Appl. Mater. Interfaces*, 2021, **13**, 18380–18388.
116 X. Wang, S. F. Seyedpour, S. Hrapovic, U. D. Hemraz, M. Mozafari, M. Soroush, M. A. Islam, A. Mollahosseini, M. Sadrzadeh and J.-Y. Cho, *Clean. Eng. Tech.*, 2025, **27**, 100999.
117 X. Zhang, X. Bai, Y. Wang, F. Hu, X. Lu and J. Li, *J. Membr. Sci.*, 2024, **692**, 122290.
118 S. Xie, X. Tan, Z. Xue, P. Geysens, H. Pan, W. Guo, Z. Zhou, X. Zhang, I. F. J. Vankelecom and J. Fransaer, *Angew. Chem., Int. Ed.*, 2024, **63**, e202401817.
119 S. Jeong, J. Jeong, S. Lim, W. Kim, H. Kwon and J. Kim, *Chem. Eng. J.*, 2024, **481**, 148294.
120 J. Wan, M. Nian, C. Yang, K. Ge, J. Liu, Z. Chen, J. Duan and W. Jin, *J. Membr. Sci.*, 2022, **642**, 119991.
121 Z. Liu, H. Zhao, B. Hua, Y. Wang, T. Lu, M. Guo, G. Dong, J. Zhu and Y. Zhang, *ACS Appl. Mater. Interfaces*, 2025, **17**, 6867–6877.
122 J. Zhang, X. Sun, J. Xin, L. Wang, Y. Fan, J. Zheng, S. Li, J. Xu, N. Li and S. Zhang, *ACS Sustain. Chem. Eng.*, 2025, **13**, 2368–2379.
123 Y. Cui, X. Cui, G. Yang, P. Yu, C. Wang, Z. Kang, H. Guo and D. Xia, *J. Membr. Sci.*, 2024, **689**, 122174.
124 J. J. Teesdale, M. Lee, R. Lu and Z. P. Smith, *J. Am. Chem. Soc.*, 2023, **145**, 830–840.
125 C. Wang, Y. Sun, L. Li, R. Krishna, T. Ji, S. Chen, J. Yan and Y. Liu, *Angew. Chem., Int. Ed.*, 2022, **61**, e202203663.
126 J. Yan, Y. Sun, T. Ji, C. Zhang, L. Liu and Y. Liu, *J. Membr. Sci.*, 2022, **653**, 120496.
127 T. Lee, A. Ozcan, I. Park, D. Fan, J. Jang, P. G. M. Mileo, S. Yoo, J. Roh, J. Kang, B. Lee, Y. Cho, R. Semino, H. Kim, G. Maurin and H. Park, *Adv. Funct. Mater.*, 2021, **31**, 2103973.
128 T. D. Bennett and A. K. Cheetham, *Acc. Chem. Res.*, 2014, **47**, 1555–1562.
129 J. Kang, X. Yang, Q. Hu, Z. Cai, L. M. Liu and L. Guo, *Chem. Rev.*, 2023, **123**, 8859–8941.
130 Z. Lin, J. J. Richardson, J. Zhou and F. Caruso, *Nat. Rev. Mater.*, 2023, **7**, 273–286.
131 J. Fonseca, T. Gong, L. Jiao and H. Jiang, *J. Mater. Chem. A*, 2021, **9**, 10562–10611.
132 J. M. Tuffnell, C. W. Ashling, J. Hou, S. Li, L. Longley, M. L. Rios Gomez and T. D. Bennett, *Chem. Commun.*, 2019, **55**, 8705–8715.
133 H. Mahdavi, F. Zadehahmadi, M. Arzani, L. Melag, A. L. Sutton, M. M. Sadiq, Z. Xie, M. R. Hill and B. D. Freeman, *Adv. Mater.*, 2025, e05579.
134 M. Kim, H.-S. Lee, D.-H. Seo, S. J. Cho, E.-c. Jeon and H. R. Moon, *Nat. Commun.*, 2024, **15**, 1174.
135 Y. Feng, W. Yan, Z. Kang, X. Zou, W. Fan, Y. Jiang, L. Fan, R. Wang and D. Sun, *Chem. Eng. J.*, 2023, **465**, 142873.
136 D. Li, Z. Yang, L. Yang, C. Ma, M. Ye, Y. Sun, Z. Qiao and A. Chen, *J. Membr. Sci.*, 2024, **695**, 122492.
137 S. Li, C. Ma, J. Hou, S. Yu, A. Chen, J. Du, P. A. Chater, D. S. Keeble, Z. Qiao, C. Zhong, D. A. Keen, Y. Liu and T. D. Bennett, *Nat. Commun.*, 2025, **16**, 1622.
138 Y. Wang, H. Jin, Q. Ma, K. Mo, H. Mao, A. Feldhoff, X. Cao, Y. Li, F. Pan and Z. Jiang, *Angew. Chem., Int. Ed.*, 2020, **59**, 4365–4369.
139 H. Xia, H. Jin, Y. Zhang, H. Song, J. Hu, Y. Huang and Y. Li, *J. Membr. Sci.*, 2022, **655**, 120611.
140 Y. Zhang, Y. Wang, H. Xia, P. Gao, Y. Cao, H. Jin and Y. Li, *Chem. Commun.*, 2022, **58**, 9548–9551.
141 N. Li, C. Ma, Z. Wang, D. Li, Z. Qiao and C. Zhong, *J. Membr. Sci.*, 2025, **715**, 123453.

142 M. Y. B. Zulkifli, K. Su, R. Chen, J. Hou and V. Chen, *Adv. Membr.*, 2022, **2**, 100036.
143 A. M. Chester, C. Castillo-Blas, L. Wondraczek, D. A. Keen and T. D. Bennett, *Chem. Eur. J.*, 2022, **28**, e202200345.
144 Z. Li, Y. Wang, J. Zhang, S. Cheng and Y. Sun, *Membranes*, 2024, **14**, 1–18.
145 R. Lin, M. Chai, Y. Zhou, V. Chen, T. D. Bennett and J. Hou, *Chem. Soc. Rev.*, 2023, **52**, 4149–4172.
146 N. Ma and S. Horike, *Chem. Rev.*, 2022, **122**, 4163–4203.
147 B. Hosseini Monjezi, K. Kutonova, M. Tsotsalas, S. Henke and A. Knebel, *Angew Chem. Int. Ed. Engl.*, 2021, **60**, 15153–15164.
148 S. Yang, V. V. Karve, A. Justin, I. Kochetygov, J. Espín, M. Asgari, O. Trukhina, D. T. Sun, L. Peng and W. L. Queen, *Coord. Chem. Rev.*, 2021, **427**, 213525.
149 L. Hu, W.-I. Lee, S. Roy, A. Subramanian, K. Kisslinger, L. Zhu, S. Fan, S. Hwang, V. T. Bui, T. Tran, G. Zhang, Y. Ding, P. M. Ajayan, C.-Y. Nam and H. Lin, *Nat. Commun.*, 2024, **15**, 5688.
150 T. Lee, B. Lee, S. Yoo, H. Lee, W. Wu, Z. P. Smith and H. Park, *Nat. Commun.*, 2023, **14**, 8330.
151 P. Su, S. Chen, L. Chen and W. Li, *J. Membr. Sci.*, 2024, **691**, 122246.
152 H. Zhang, R. Zou and Y. Zhao, *Coord. Chem. Rev.*, 2015, **292**, 74–90.
153 T. Xu, B. Wu, W. Li, Y. Li, Y. Zhu, F. Sheng, Q. Li, L. Ge, X. Li, H. Wang and T. Xu, *Sci. Adv.*, 2024, **10**, eadn0944.
154 Q. Xin, J. Dong, W. Shao, X. Ding, N. Gao, L. Zhang, H. Jin, H. Chen and Y. Zhang, *J. Membr. Sci.*, 2025, **714**, 123431.
155 X. Yang, Q. Zhang, Y. Liu, M. Nian, M. Xie, S. Xie, Q. Yang, S. Wang, H. Wei, J. Duan, S. Dong and H. Xing, *Angew. Chem., Int. Ed.*, 2023, **62**, e202303280.
156 Z. Li, T. Li, W. Zheng, X. Li, J. Zhu, M. Yu, X. Jiang, X. Wu, G. He and J. Zhang, *J. Membr. Sci.*, 2025, **717**, 123657.
157 Z. Qin, J. Wei, Y. Wu, M. Deng, L. Yao, L. Yang, W. Jiang, J. Zheng, Z. Liu and Z. Dai, *Results Eng.*, 2024, **24**, 103184.
158 A. Sabetghadam, X. Liu, S. Gottmer, L. Chu, J. Gascon and F. Kapteijn, *J. Membr. Sci.*, 2019, **570**, 226–235.
159 Y. Cheng, X. Wang, C. Jia, Y. Wang, L. Zhai, Q. Wang and D. Zhao, *J. Membr. Sci.*, 2017, **539**, 213–223.
160 C. Zhu, Y. Peng, K. Li, L. Liu and W. Yang, *J. Membr. Sci.*, 2024, **709**, 123140.
161 Y. Sun, J. Yan, Y. Gao, T. Ji, S. Chen, C. Wang, P. Lu, Y. Li and Y. Liu, *Angew. Chem., Int. Ed.*, 2023, **62**, e202216697.
162 Q. Wang, Y. Tang, L. Liu, C. Liu, K. Zhang, X. Tian, X. Feng, R. Zhang, Y. Yu and T. Gu, *J. Membr. Sci.*, 2025, **726**, 124067.
163 C. Chuah, K. Goh, Y. Yang, H. Gong, W. Li, H. E. Karahan, M. D. Guiver, R. Wang and T. Bae, *Chem. Rev.*, 2018, **118**, 8655–8769.
164 L. M. Robeson, *J. Membr. Sci.*, 2008, **320**, 390–400.
165 Y. Feng, Q. Chen, M. Jiang and J. Yao, *Ind. Eng. Chem. Res.*, 2019, **58**, 17646–17659.
166 Z. Gu, X. Zhang, R. Liang, F. Wang, D. Wang, A. Chen and Z. Qiao, *ACS Appl. Polym. Mater.*, 2025, **7**, 11890–11900.
167 Y. Liang, Z. Zhang, A. Chen, C. Yu, Y. Sun, J. Du, Z. Qiao, Z. Wang, M. D. Guiver and C. Zhong, *Angew. Chem., Int. Ed.*, 2024, **63**, e202404058.
168 C. Yu, X. Cen, Z. Zhang, Y. Sun, W. Xue, Z. Qiao, M. D. Guiver and C. Zhong, *Adv. Mater.*, 2023, **35**, 2307013.
169 C. A. Mirkin, S. H. Petrosko, N. Artzi, K. Aydin, A. Biaggne, C. J. Brinker, K. E. Bujold, Y. C. Cao, R. R. Chan, C. Chen, P.-C. Chen, X. Chen, O. J. G. L. Chevalier, C. H. J. Choi, R. M. Crooks, V. P. Dravid, J. S. Du, S. B. Ebrahimi, H. Fan, O. K. Farha, C. A. Figg, T. D. Fink, C. M. Forsyth, H. Fuchs, F. M. Geiger, N. C. Gianneschi, K. J. Gibson, D. S. Ginger, S. Guo, J. S. Hanes, L. Hao, J. Huang, B. M. Hunter, F. Huo, J. Hwang, R. Jin, S. O. Kelley, T. J. Kempa, Y. Kim, S. Kudruk, S. Kumari, K. M. Landy, K.-B. Lee, N. J. Leon, J. Li, Y. Li, Z. Li, B. Liu, G. Liu, X. Liu, L. M. Liz-Marzán, J. H. Lorch, T. Luo, R. J. Macfarlane, J. E. Millstone, M. Mrksich, C. J. Murphy, R. R. Naik, A. E. Nel, C. Oetheimer, J. K. Hedlund Orbeck, S.-J. Park, B. E. Partridge, N. A. Peppas, M. L. Personick, A. Raj, N. Ramani, M. B. Ross, S. B. Ross, E. H. Sargent, T. Sengupta, G. C. Schatz, D. S. Seferos, T. Seideman, S. E. Seo, B. Shen, W. Shim, D. Shin, U. Simon, A. J. Sinegra, P. T. Smith, A. M. Spokoyny, P. J. Stang, A. H. Stegh, J. F. Stoddart, D. F. Swearer, W. Tan, M. H. Teplensky, C. S. Thaxton, D. R. Walt, M. X. Wang, Z. Wang, W. D. Wei, P. S. Weiss, P. H. Winegar, Y. Xia, Y. Xie, X. Xu, P. Yang, Y. Yang, Z. Ye, K. R. Yoon, C. Zhang, H. Zhang, K. Zhang, L. Zhang, X. Zhang, Y. Zhang, Z. Zheng, W. Zhou, S. Zhu and W. Zhu, *ACS Nano*, 2025, **19**, 31933–31968.
170 C.-C. Lin, E. Parrish and R. J. Composto, *Macromolecules*, 2016, **49**, 5755–5772.
171 J. Huang, J. Zhou and M. Liu, *JACS Au*, 2022, **2**, 280–291.
172 T. Lee, J. Jang, B. Lee, W.-N. Wu, Z. P. Smith and H. B. Park, *Macromolecules*, 2024, **57**, 11242–11250.
173 S. K. Kumar, B. C. Benicewicz, R. A. Vaia and K. I. Winey, *Macromolecules*, 2017, **50**, 714–731.
174 Y. Chen, W. Lu, M. Schroder and S. Yang, *Acc. Chem. Res.*, 2023, **56**, 2569–2581.
175 Ü. Kökçam-Demir, A. Goldman, L. Esrafili, M. Gharib, A. Morsali, O. Weingart and C. Janiak, *Chem. Soc. Rev.*, 2020, **49**, 2751–2798.
176 J. E. Bachman, Z. P. Smith, T. Li, T. Xu and J. R. Long, *Nat. Mater.*, 2016, **15**, 845–849.
177 H. Demir, H. Daglar, H. C. Gulbalkan, G. O. Aksu and S. Keskin, *Coord. Chem. Rev.*, 2023, **484**, 215112.
178 X. Cheng, Y. Liao, Z. Lei, J. Li, X. Fan and X. Xiao, *J. Membr. Sci.*, 2023, **672**, 121430.
179 Z. Zhang, X. Cao, C. Geng, Y. Sun, Y. He, Z. Qiao and C. Zhong, *J. Membr. Sci.*, 2022, **650**, 120399.
180 Z. Zheng, O. Zhang, C. Borgs, J. T. Chayes and O. M. Yaghi, *J. Am. Chem. Soc.*, 2023, **145**, 18048–18062.
181 Z. Zheng, Z. Rong, N. Rampal, C. Borgs, J. T. Chayes and O. M. Yaghi, *Angew. Chem., Int. Ed.*, 2023, **62**, e202311983.
182 A. Ozcan, F. X. Coudert, S. M. J. Rogge, G. Heydenrych, D. Fan, A. P. Sarikas, S. Keskin, G. Maurin, G. E. Froudakis, S. Wuttke and I. Erucar, *J. Am. Chem. Soc.*, 2025, **147**, 23367–23380.